Performance Impact of Ion Sources in Inertial Electrostatic Confinement Devices

By

Alexandru D. Calburean

SUBMITTED TO THE DEPARTMENT OF NUCLEAR SCIENCE AND ENGINEERING IN PARTIAL FULFILLMENT OF THE REQUIREMENTS FOR THE DEGREE OF

BACHELOR OF SCIENCE IN NUCLEAR SCIENCE AND ENGINEERING AT THE
MASSACHUSETTS INSTITUTE OF TECHNOLOGY

February 2020

Signature of Author:_____

Alexandru Calburean
Department of Nuclear Engineering
May 16, 2019

Certified by:_____

Anne White
Cecil and Ida Green Professor in Nuclear Engineering
Thesis Supervisor

Certified by:_____

Andrew Seltzman
Postdoctoral Associate
Thesis Supervisor

Accepted by:_____

Michael Short
Professor of Nuclear Science and Engineering
Chairman, NSE Committee for Undergraduate Students

Performance Impact of Ion Sources in Inertial Electrostatic Confinement Devices

by

Alexandru D. Calburean

Submitted to the Department of Nuclear Science and Engineering on May 16, 2019
In partial Fulfillment of the Requirements for the Degree of
Bachelor of Science in Nuclear Science and Engineering

ABSTRACT

In order to improve the performance of Inertial Electrostatic Confinement (IEC) based fusion devices, so as to improve their effectiveness as low cost, portable neutron sources, a novel use of ion sources is proposed as a means of increasing fusion reaction rate at similar power levels. This paper aims to determine the success and practicality of the proposed use type for ion sources and characterize the IEC device in question, in terms of performance, and neutron emission. The application outlined aims to improve upon the performance of IEC devices with an anode layer ion source. The above-mentioned approach was evaluated by first conditioning the IEC fusion device in question. Then a neutron flux baseline was recorded as a metric for performance, and to evaluate the assumption of neutron emission isotropy in the device. Then an ion source was installed in the chamber, and the system was once again conditioned in the same manner. A similar baseline reading and analysis was done to ensure a correct comparison could be made between performance with the ion source turned on and off. Next the system was run with the ion source at full power to allow for further characterization of the performance and stability of the device. Finally, a last run was carried out with the ion source properly tuned, and results were compared to both baseline runs. It has been shown that there is a potential performance gain from operation with an ion source, both in terms of system stability and improved neutron emission. Across all run campaigns, the assumption of isotropic emission was shown to be a poor representation of the actual emission. With a higher degree of certainty, it has been shown that operation with an ion source serves to reliably exaggerate the anisotropy found in baseline campaigns.

Thesis Supervisor: Anne White
Title: Cecil and Ida Green Professor in Nuclear Engineering

Thesis Supervisor: Andrew Seltzman
Title: Postdoctoral Associate

1. Introduction

1.1 Overview of Concept

Inertial electrostatic confinement (IEC) is a fusion concept in which deuterium ions are accelerated toward and recirculated through a central electric field, during which fusion occurs. The typical IEC construction is as follows: A main core consisting of an electrically grounded stainless-steel outer vacuum chamber, often spherical, and an inner accelerating "grid." This grid structure is a geodesic sphere made up of several stainless-steel rings. It is biased at a high negative voltage (up to -40kV) and contains multiple openings such that ion collisions with this grid structure are minimized. In some cases, IEC systems are run with ion sources, usually of the hot filament type due to simplicity, to allow for increased current draw and thus higher total neutron flux, and to allow for more stable operation, usually below the Paschen minimum. The vacuum in the system is maintained by a fore pump coupled to a high vacuum pump, in this case it is a turbomolecular drag pump, backed by a rotary vane pump. The system is powered by a high voltage power supply, in this case, this is a Spellman PVT series supply capable of -40kV at a constant 5mA. The mounted ion source is an anode layer ion source type from Technical Plasmas LLC. Finally, neutron detection in this case is done with a BTI PND bubble detector of sensitivity ~22 bubbles / mrem.

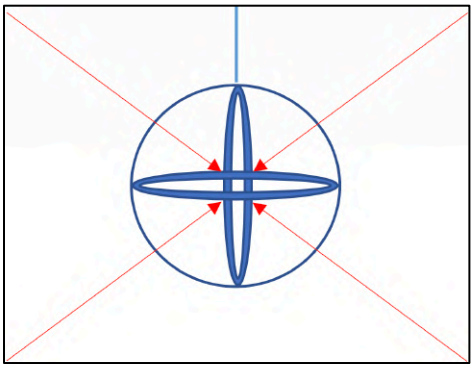

Figure 1. The ideal ion trajectory in IEC systems. The blue spherical structure is the grid, biased at a high negative voltage; the red arrows are the ideal ion trajectories.

1.2 Applications of IEC devices

Due to the simple construction, IEC devices can be constructed and used inexpensively, rapidly, and extensively as portable and tunable source for high energy neutrons, protons, and x-rays. Unlike a sealed neutron tube, the system is very easy to open and work on, and requires minimal conditioning to return to full power. Unlike neutron generation by radioactive sources such as Am-Be or Pu-Be sources, the IEC scheme contains no radioactive material, and emits no radioactive byproducts, thereby eliminating several key risk factors in source deployment. More importantly, it can be turned off when not in use. Further, runaway conditions in the IEC machine can only result in the destruction of the machine itself at worst. For these reasons, an industrial IEC based neutron generator is not only attractive, but a marked improvement over current preferred neutron sources.

1.3 Motivation for Work and Goal of Research

IEC systems have very versatile applications as mentioned above; therefore, further improvement in device performance and neutron output is desirable to enhance those uses. Previous work indicated that improvement of the efficiency of IEC machines was possible with reduction of charge exchange [2]. In this paper increasing the number of ions present relative to neutrals is considered as a method of decreasing charge exchange. To this end hardware tests needed to be carried out to verify whether this approach to the reduction of charge exchange was successful as a means of improving the neutron output of the device. Further, because the particular device investigated in this paper was never before characterized, another goal of the work was to carry out such characterization of the baseline neutron output of the device.

To that end, the work presented in this thesis will summarize whether increased ion amount relative to neutrals, achieved via an anode layer ion source, will noticeably increase fusion rate in IEC machines as measured by neutron output. This will be done by comparison of isotropic neutron flux as measured by BTI PND bubble dosimeters placed at various points along a circumference around the machine during operation with and without ion sources. Both positive and negative results will allow for further understanding of the magnitude of losses that occur during regular IEC operation. The same work will also serve to characterize the performance and neutron flux of the MIT Compact Classroom Fusion Device (CCFD). Since this is a device, which has not yet undergone reaction rate benchmarking, the extensive operation of the device required for this work provides the excellent opportunity for the establishment of such benchmarks, as outlined above.

1.4 Design Details

1.4.1 The Vacuum System

There are several concepts to note here about the ideal system. For simplicity, each system of the machine can be considered separately. To begin, the vacuum system creates the necessary conditions for sustaining a plasma discharge, such a system should be run with a scroll or diaphragm pump coupled to a turbo-drag pump to prevent oil fouling of the main chamber. In this case an oil sealed fore pump and turbo drag pump are used with long bent vacuum plumbing. Because of this, oil fouling is considered to be minimal.

$$Knudsen\ Number = \frac{Mean\ Free\ Path}{Diameter} \tag{1.1}$$

In the case of the system described in this work, the foreline is at approximately 100mTorr, in a 1-inch diameter line. This results in a Knudsen Number of approximately 9.4E-5 for oil molecules of 1.7 angstroms in size. For Knudsen number less than 0.5, the flow type is viscous. This means that the oil in the foreline is in viscous flow and thus the oil molecules that result from the pump back streaming are unable to make their way into the chamber. From the oil sealed pump, the foreline continues into a Varian V250 turbo drag pump.

1.4.2 The Power Supply

The next consideration is the power supply. Neutron flux scales with both voltage, via increased fusion cross section, and current via increased collision frequency. Fusion Cross section scales with voltage because ion energy scales with voltage. Ion energy scales with voltage applied to the grid occurs because the deuteron is accelerated according to the electric field present from the inner grid. This means that the larger the voltage on the grid is, the larger the electric field is, and the more energy the ion is able to pick up. As is seen below, for ion energies below 200keV deuterium – deuterium fusion cross section strongly scales with deuteron energy. Similarly, the total reaction rate depends on the number of ions that are able to participate in fusion collisions. The number of ions that can be supported in the machine is proportional to current. Experimentally, the fusion rate was found to scale linearly with ion current [4]. Therefore, the ideal power supply for industrial use would allow for around 200kV operation at 100's of mA. Figure 2 below shows the fusion cross section for beam target experiments. The fusor experiences both beam beam and beam target fusions.

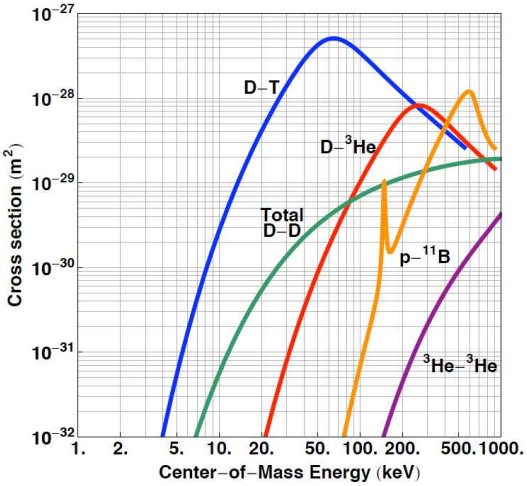

Figure 2. A visualization of fusion cross section for beam on target experiments[7].

As can be seen figure 2, there is little to gain from increasing voltage past 200kV for deuterium-deuterium fusion cross section, and there is loss in cross for deuterium-tritium fusion. Further, increase in voltage comes with increased danger in the form of massively increased x-ray production. In addition, operation beyond even 100kV comes with engineering challenges, such as designing a high voltage vacuum feedthrough that isn't plagued by electrical instability and electromagnetic interference (EMI) generation due to corona emission. For the machine described in this work, 40kV at 5mA was experimentally verified in prior work to be sufficient for the production enough neutrons in a 10-minute run to ensure that the BTI detectors will pick up the emission. Therefore, the 40kV supply is adequate, and ideal for this study, as there are no excessive electrical engineering challenges and x-ray emissions. To compensate for low current, run times are kept as long as possible, at about 10 minutes. In an industrial system, to maximize flux, a 200kV capable supply with many 100's of mA running in a deuterium-tritium system would be ideal. Additionally, in such large systems, active cooling of components is required for long term operation. This was another reason why a low current supply is favorable, because active cooling presents another layer of complexity beyond the scope of this work.

1.4.3 The Fuel Metering System

A fuel metering system was designed to allow for two key abilities. First, the system was designed to be remote controlled, and second, the system was designed to remain stable over the duration of a run. The first goal was achieved by collecting sensor information through a national instruments usb 6001 DAQ, and using analog outputs to send back control commands to the system. The second goal was accomplished with the ability for system pressure to self-regulate in order to achieve stability. This was done through a LabVIEW PID controller VI, that was tuned to the system, and was used to control the valve position on a mass flow controller. The mass flow controller draws from a bottled deuterium of 99.8% purity.

1.4.4 The Data Collection System.

Pressure was collected by the LabVIEW VI, while power supply voltage and current, ion source voltage, and neutron measurements were collected by hand. The pressure was logged by LabVIEW because it is required for the rapid response PID controller component of the VI. The rest of the quantities were collected by hand because they showed little change over run periods and were easy to track by hand. Neutron detection was handled by 6 BTI PND fast neutron bubble dosimeters, calibrated in the 21-23 bubbles/mrem range. The neutron detection solution was chosen specifically because it is impervious to EMI and the low cost allows for multiple detectors to be set up around a radius for reduction of measurement error, and tracking of the assumed isotropy of the system's neutron flux.

1.4.5 The Ion Source System

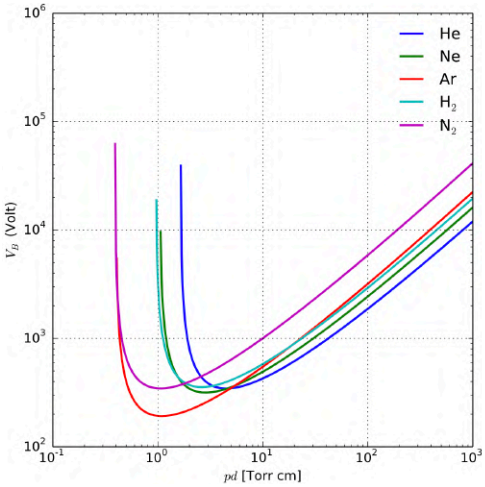

Figure 3. Paschen Curves obtained for helium, neon, argon, hydrogen, and nitrogen [6].

To understand the usefulness of ion sources, consider the general case of Paschen's law above. As the pressure term in Paschen's law decreases, the voltage required to maintain a glow discharge rapidly increases. The case shown above is for parallel plate geometry, whereas the fusor described in this work is closer to a hollow cathode geometry. This change in geometry serves to dampen the climb of voltage requirement on the left hand side of Paschen's law [3].

As the fusor operates in the glow discharge regime it is governed by Paschen's law. This means that all the system parameters feedback on one another. For example, a change in pressure will change the voltage that the chamber can accommodate, and the current that the system draws. It is primarily through this mechanism that ion source-less systems are controlled. For the deuterium atmosphere that the fusor runs with, and a pressure * distance term on the order of .01 Torr cm, the fusor runs at 40kV with a 5mA current limit on the supply. To further increase voltage, a pressure decrease is required, but this in turn starves the fusor of ions, which serves to stop the glow discharge.

The total amount of ionization depends on the amount of neutrals present to be ionized and the applied voltage and pressure [9], which is why decreasing pressure in the fusor, without increasing voltage stops the glow discharge. To allow this pressure drop, an ion source is mounted to supply additional ions to the fusor. Drop in pressure is required in this particular experiment to reduce the amount of neutrals present in the fusor. Additionally, operating a fusor slightly below the Paschen minimum, where slightly is defined as the point where pressure is lowered while voltage and current was limited exactly to the point where the glow discharge extinguishes, i.e. there is no more current draw on the supply, is useful because the system parameters are now able to be adjusted more quickly, by regulating the power to the ion source, instead of a relying on power regulation through pressure, which for large systems has significant hysteresis.

When a glow discharge begins, an IEC machine goes from an essentially perfect insulator to almost a perfect conductor in a very short timeframe [9]. This quick voltage rise time can destroy power supplies and create arcing damage if not properly controlled. Further, oscillations in system variables that result from an intermittent glow discharge, like outgassing due to plasma bombardment, can make the system uncontrollable. To prevent such sudden power switching or interruptions (in the case negative pressure spikes), an ion source may be mounted to allow for a steady stream of ions to be produced and therefore allow for a stable glow discharge beyond the point that could be maintained with just a single grid, as mentioned above. An ion source could be as simple as a heated copper wire, which creates ions through electron collisions that are generated by thermionic emission, or as complex as a hall effect ion source. A prepackaged solution (an anode layer ion source) was chosen in this case to save time.

The IEC device operates on the principle that when neutral deuterium gas is fed, the high potential difference between the outer grounded chamber and the inner grid, results in discharge ionization and a plasma corresponding to the criteria of the Paschen curve is formed. The newly formed, positive, deuterium ions are accelerated toward the inner grid, once inside this region, the ions are now shielded from the electric field and collide under their own inertia, and given that it is high enough, fusion occurs. This is the ideal mode of operation, but previous work has shown that significant fusion occurs with the deuterium ions against the background [12]. This results from the cases where the ions pass through the inner grid without colliding. This case is the dominant case, resulting in ion scattering, charge exchange, and wall deposition. Secondary electrons emitted from the grid then result in bremsstrahlung x-rays and heating of the vacuum vessel.

The case of charge exchange is particularly troubling as it creates fast neutrals that have a high probability of engaging in further charge exchange. These fast neutrals are essentially what leads to wall heating, as the electric field cannot slow them down. The further an ion gets in the opposite direction from the grid, the more it will slow as a result of being pulled back by the grid's electric field. If the mean free path of the ion is large enough, ion recirculation may occur resulting in another pass at fusion by acceleration towards the inner grid [10].

Because IEC systems are bound by the Paschen curve, operation outside of the parameters outline by the curve result in an unstable system, and because the Paschen curve becomes exponential as a technical vacuum tends to high vacuum, extreme instability, including permanent plasma extinguishing as well intermitted extinguishing can occur [2]. This has the consequence of keeping the system in a quickly changing transient state that is hard to stabilize or change. The effect of unstable operation further imposes the problem of electrical noise, which can be a severe problem for the many high input impedance detectors used. To address the above concerns (reduction of charge exchange, possibility of operation below the Paschen minimum, to improve probability of fusion) as well as to allow for more stable operation, ion sources can be mounted and their emission precisely varied to allow for further tuning of the system.

2. Literature Review

2.1 Charge Exchange

Work with IEC machines thus far has largely been done on the amateur level or via small university research programs. It is because of this small-scale nature of IEC research, that some of the finer details of IEC operation have not yet been worked out. One such detail is the mechanics of charge exchange inside the fusor. While some papers acknowledge its existence as a contributing loss mode, it is rare that a full paper is devoted to quantifying models and validating hypotheses in this area. Such an effort is detailed by Gabriel Becerra et al from the university of Madison Wisconsin's IEC group, in a presentation for the US-Japan IEC conference of 2015[1]. The group constructed a neutral particle analyzer and deployed it in search of charge exchange behavior in the fusor. They report a very large peak of neutrals present at 100keV in their 100kV machine [1]. This implies that lots of ions are losing essentially all their energy very close to the grid, as the high energy neutrals are being created as a result of collisions with very high energy ions.

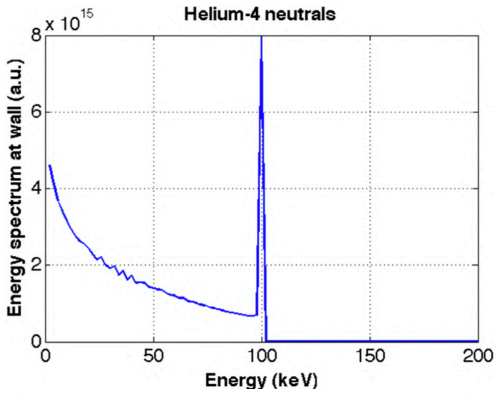

Figure 4. A graphical representation of measured neutral energies in the University of Madison Wisconsin IEC neutral particle analyzer study [1].

Figure 4 above, shows the relative population of 100keV neutrals from this study. This combined with the understanding that charge exchange reactions have a cross section orders of magnitude higher than fusion cross sections begins to quickly paint the picture of just how bad this loss mechanism is for the fusor. Figure 5 below from the same group shows a visual depiction of these measured charge exchange cross sections relative to each other for various fusion gasses. It should be noted that they are of much higher magnitude than fusion cross sections.

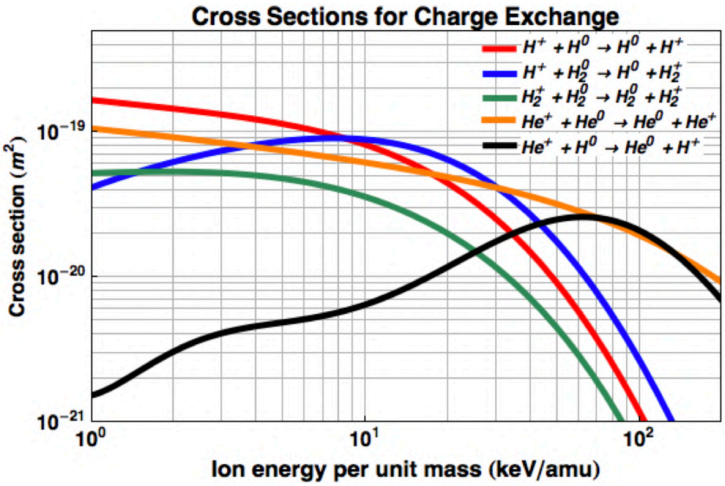

Figure 5. Measured charge exchange cross sections from University of Madison Wisconsin IEC neutral particle analyzer study [1].

This is very important for the following reason. Suppose that the electric field in a typical IEC machine is modeled generally as a spherical capacitor. A case for this is given by [16] The equation that describes the electric field is as follows [16].

$$(V = \frac{-2V_0\, ab}{(b-a)r} + \frac{2V_0\, a}{(b-a)} + V_0\,) \tag{1.2}$$

where a is the radius of the inner grid and b is the radius of the outer grid, both considered as constants, and r is the point at which the field is being considered. Further the equations that describe the acceleration of fuel ion are as follows:

$$F = q_{ion}E \tag{1.3}$$

$$F = m_{ion}a \tag{1.4}$$

$$a = \frac{q_{ion}E}{m_{ion}} \tag{1.5}$$

The acceleration of an ion tracks the electric field, and the electric field decays rapidly (with radius to the second power) over the chamber diameter, it then becomes a very problematic if an ion experiences a charge exchange reaction near the grid, as it has essentially no time to pick up enough additional energy to collide with sufficient energy once it reaches the inner grid to fuse. The closer an ion experiences its last charge exchange event to the grid, before it continues simple linear motion towards the inner grid, the less energy that ion will have by the time crosses into the inner part of the grid, where no more electrostatic acceleration occurs and fusion is done as a result of the particles' momentum. If charge exchange reactions were very common right outside the edge of grid, where plasma density is the highest [12], this configuration would result in the highest ion energy loss, and would be a massive decrease in fusion cross section by lowering v_{ion} . This seems to be the case as some of the currently published work on charge exchange states the following.

Spectroscopic analysis of ion channel emissions of IEC machines done by S Collis and J Khachan indicate that ions on average see only about 20% of the full potential well depth in ion channels [5]. This suggests that even in focused ion channels (that form due to electrostatic lensing), i.e. a location where one would expect concentrated ion population relative to the background, ions are only seeing a small fraction of the total grid applied voltage, lowering cross section and thus lowering neutron output of IEC machines. So, building a lens i.e. grid, that is better at focusing ions doesn't really solve the problem if there is significant neutral concentration in the pressure.

2.2 Prior Work

Classically the solution to combat charge exchange would be to lower pressure, this would increase the mean free path and reduce collision probability between ions and neutrals [2]. This is not the best way to go about this, as by reducing pressure, non-ion sourced fusors become ion starved and extinguish i.e. the reaction halts. Theoretically, the solution would be to feed in only ions into the machine, and used a cooled grid such as the one designed by Andrew Seltzman in [14] to reduce thermionic electron emission to inhibit ion electron recombination and thus the formation of additional neutral particles. Because this would require the use of complicated magnet arrangements for ion diversion into main chamber and further vacuum and power equipment, it would add tremendous complexity. A more reasonable solution, especially for a compact system, would be the improvement of ion concentration through the addition of ion sources. This would reduce the number of neutrals present per unit pressure and therefore reduce the charge exchange cross section. Simply stated, for a given pressure, the greater the ion partial pressure, and the lower the neutral partial pressure, the higher we expect the fusion cross section to be.

Additionally, one may consider the following, if the fusion cross section is expressed as follows from equation below, then a few advantages of running an ion sourced IEC machine become apparent.

$$\sigma_{fusion} = n_{ion} v_{ion} \tau_{ion+ion_{fusion}} \quad (1.5)$$

Most apparent are the benefits mentioned above from having increased n_{ion}, as increased n_{ion} for a given pressure mean a decrease in $n_{neutral}$. This in turn leads to a decreased charge exchange cross section, but in addition to that, fusion cross section directly scales with n_{ion} therefore it is advantageous to increase the ion population. Next, v_{ion} would also see an increase from a decrease in the amount of $n_{neutral}$, which would in turn result in a decrease of the charge exchange reaction cross section thus resulting in decrease of v_{ion} losses. The v_{ion} losses via charge exchange, as mentioned above in the work by Collis and Khachan, are found to be extremely significant. The last benefit isn't as clear cut as it comes at a cost, by running at a lower pressure, as made possible with the addition of an ion source, the amount of charge exchange can be reduced. This comes at the cost of less fuel available for the reaction and an increase in $\tau_{ion+ion_{fusion}}$ as the mean free path increases, and thus the distance until an ion-target collision can occur. There are a few things to note about the following drawbacks, first it is important to note that typically IEC machines flush most fuel out of the system through the high vacuum pump before it even has a chance to fuse; this is ultimately due to the low probability of fusion. This implies that a reduction of fuel pressure won't be an extreme problem if reduction in fuel pressure means that what fuel remains has a higher probability of being used. Thanks to a decrease in charge exchange with pressure [8], we indeed see this increase in fusion probability and thus fuel utilization, however small. Further, an increase in the mean free path does result in an increase of $\tau_{ion+ion_{fusion}}$ but adds the benefit of improved ion recirculation [8].

4. Experimental Setup

4.1 Construction

4.1.2 The Vacuum Pumps

The vacuum system is a supporting system, as such it was designed to support a specific operating range (0.1 to 10 mTorr) for this experiment. For this reason, it is configured thusly. First a turbo pump was selected to allow the system to pump down to 0.1 mTorr. Operation of the device doesn't occur at 0.1 mTorr, however, it is brought down to this point to evacuate whatever atmosphere enters the chamber overnight. Pumping down the chamber well below operating pressure, then backfilling with deuterium is necessary to ensure high fuel purity in the vacuum chamber. Turbo pumps are unable to pump from atmospheric pressure to high vacuum, instead they work in series with a pump that can evacuate down to where the turbo's operating range begins. To provide this backing to the turbo pump, an oil sealed rotary vane pump is used. The oil sealed pump is capped with an oil mist eliminator on its exhaust as a safety precaution against oil mist ejected from the pump. The turbo pump evacuates through a 90 degree 2.75 conflat throttling value into the chamber. This is done to allow the turbo pump to throttle back its

flow rate. This limitation of flow rate is required because pumping rate of the turbo unthrottled is much larger than the maximum output of the mass flow controller that feeds in deuterium. As such, the turbo is throttled to allow the system pressure to rise to the desired operating point (about 10mTorr D2). 10mTorr is chosen as the proper operating point from experience and Paschen's law but it should be noted that pressure determines the operational mode the device can be in i.e. Paschen's law gives minimum values for which the glow discharge will still exist, in this particular machine those values are as follows. For example, at 100's of mTorr a low voltage glow is visible, typical minimum current draw here is 5-10+ mA at a few kv. Bugle Jets appear from ~100-50 mTorr, here typical minimum current draw is ~5mA at ~5+KV.

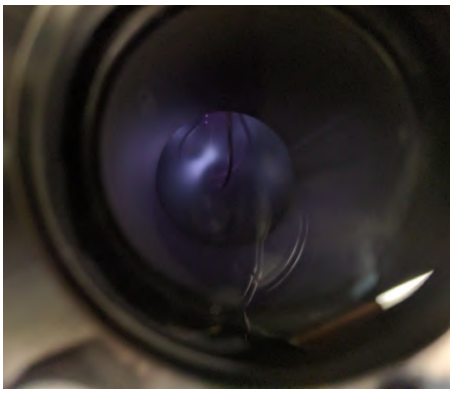

Figure 6. Nitrogen plasma in my personal device at a low voltage and high current. A bugle jet can be seen appearing from the "poissor"

A defined "poissor" is present at around 30-20 mTorr. This is a ball like region of plasma that is clearly visible in the central region of the grid. This is of higher density than surrounding regions, typical minimum current draw in this mode is about 2-5mA ~10+KV. At 20-5mTorr, an operational mode known as "star mode" appears

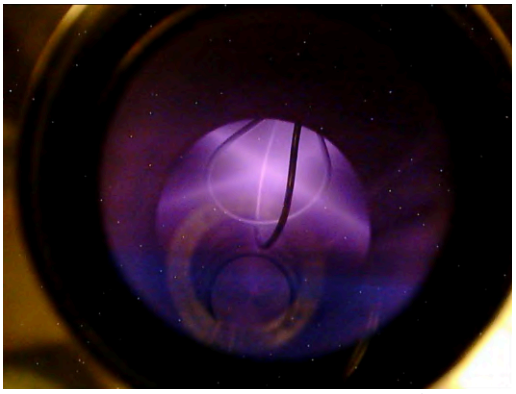

Figure 7. Deuterium Plasma star mode at 50kV with 2mA with distinct beams formed in my personal device. The image was captured with a ccd sensor, as such, x-rays registered as white dots.

In this mode, fusion occurs and power is highest. Additionally, at these pressures, voltages upwards are 30kV are possible, at which point x-ray shine through thin stainless steel that is common of vacuum chambers becomes a concern and additional shielding is needed. Typical minimum current draw in star mode ~1mA 30+kV. Of course, All these minimum current draws can be increased using ion guns.

4.1.2 The Vacuum Chamber and Shielding

The vacuum chamber consists of a 5-way NW200 304 stainless steel cross. 304 stainless steel was used because its oxide layer and smooth surface will hold less water, and won't rust over time. It is also inexpensive and inert with respect to deuterium. The top of the cross serves as the high voltage feedthrough. This is an alumina ceramic type feedthrough, chosen for its minimal outgassing compared to something like boron nitride or Teflon. The bottom of the cross is connected to a 3-foot-long NW200 diameter pipe, which features the gas feed through and a secondary pressure gauge. The front of the cross features a borosilicate viewport. The left side of the cross features a 275 series MKS convectron vacuum gauge. The right side of the chamber is originally blanked off. Later in the experiment, this flange is mounted with an ion source from technical plasmas LLC. See the figure below for a schematic of the system.

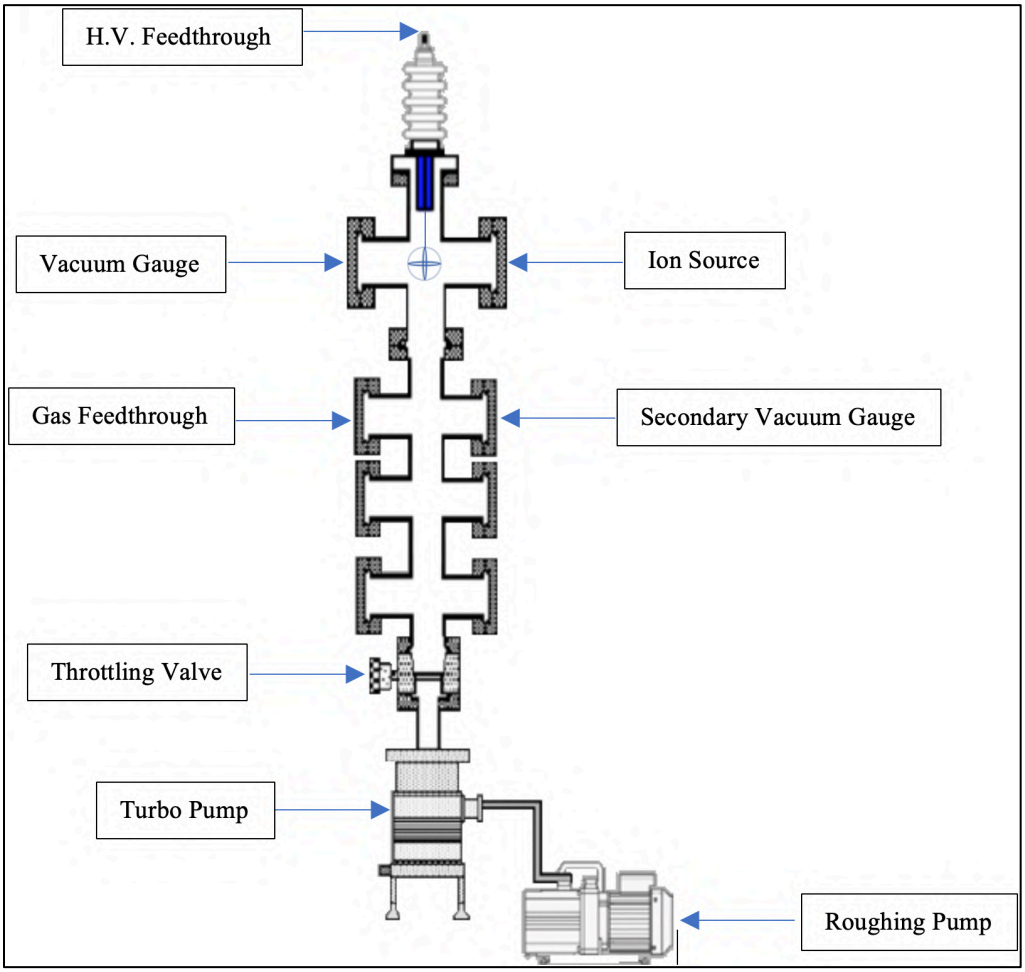

Figure 8. A graphic representation of the system assembled from modified images found in [13]

The chamber is mounted on a cart with the cross part of the chamber mounted above the surface of the cart. Because the grid is located in this section, and x-ray production was surveyed to be negligible elsewhere, only this cross location is shielded. Refer to the picture below for the shielding box. Internally, the box is lined with 1/8" thick lead sheet, and the viewport is capped with its own box during operation that is similarly lead lined. A radiation survey was conducted on this shielding, and at full power, no point of the surface of the shielding box exceeded 2mR

per hour x-ray emission. There is no shielding for neutrons because the neutron dose rate at full power is less than 2mR / hour around the device. The grid is constructed by winding thin 304 stainless steel wire around a mandrel for concentricity concerns followed by a straight bend upward to allow for mating to the high voltage feedthrough. This straight portion of the grid is not shielded and thus alters the electric field of the main spherical structure, but this is not taken to be a problem because the optical path of the ion beam aims straight in the middle of the central spherical structure of the inner grid. Other ions that are formed around the straight region of the grid will still contribute to the fusion rate, and because the structure remains the same for all run campaigns it isn't a problem.

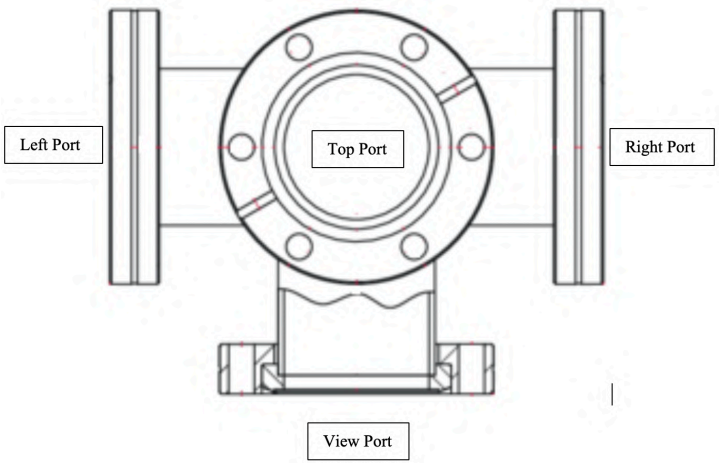

Figure 9. Image of 5 way cross that is used as the main section of the chamber, modified from [11]

4.1.3 The Gas Input System

Gas is fed to the system using a 10 SCCM mass flow controller that is electronically controlled via the main control LabVIEW VI. A 10 SCCM value was chosen because smaller mass flow rate controllers would be more easily overwhelmed by even the throttled turbo pump, and much larger mass flow rate value controllers would not allow for as fine control over system pressure. More clearly, at 10 SCCM, the low speed pumping rate of the vacuum pumps, coupled with the middle throughput ability of the mass flow controller (5 SCCM), allow she system's fuel flow balance to yield a pressure in the desired range, about 10mTorr. At lower flow rates, the pumping rate is able to overwhelm the mass flow controller, i.e. remove gas faster than what the mass flow controller can input to achieve a flow balance resulting in a 10mTorr pressure. Similarly, with much higher flow rate mass flow controllers, gas input occurs in larger quantities, meaning that fine control of operating pressure becomes more difficult. The gas system is as follows, the fuel is fed from a deuterium bottle of 99.8% purity. This fuel is fed through a ¼" Swagelok sealed stainless steel line into a gas manifold to allow for venting or other gas types for other experiments. From the gas manifold the deuterium feeds into the input of the mass flow controller at a pressure of about 15 psi gauge. The mass flow controller regulates and feeds much smaller pressure into the chamber via another stainless-steel line. The mass flow controller itself has a PID controller built in, so the PID controller output of the LabVIEW VI is used as the setpoint command for the mass flow controller's own PID controller.

4.1.4 The Power Supplies

The power to the system is supplied in a few ways. First, two separate circuits are used to power the entire system. One circuit is used to give power to pumps, I/O, sensors, and the Emco F40 dc – dc converter that powers ion source. The other is used to power the high voltage power supply. The high voltage power supply is a Spellman PVT series -40kV at 5mA supply. This supply is isolated from the rest of the circuit through isolation transformers and is fused separately. The supply has the option of being computer controlled through 0-5V analog control inputs, or manually controlled through potentiometers that allow manual adjustment of the 0-5V control signal. Both current, and voltage limits may be set. Because an unconditioned system may arc and/or experience electropolishing events that draw significant current, the supply is limited to about half voltage and current output during conditioning.

4.1.5 The Control System

The machine is controlled with a LabVIEW VI purpose built for the device, that couples to a National Instruments DAQ (usb-6001). The DAQ acquires sensor data from the power supply current and voltage monitors, pressure sensors, and flow rate sensor on the mass flow controller. The VI uses the pressure signal as part of a tuned PID control scheme for the pressure control, and the analog output functionality of the DAQ as a means of feeding the control point to the mass flow controller. This in turn allows for the adjustment of pressure, and through Paschen's law, adjustment of current and voltage values of the supply. It should be noted that the high voltage supply is controlled manually using the front panel potentiometers. These potentiometers don't fix voltage and current values, rather they set limits on the upper level these values may reach. Ultimately system pressure and later ion source power are used to control the fusor. Refer to the figure below for a detailed view of the control front panel. The following figure shows the LabVIEW control output. The right graph shows live system pressure as a white line, and the desired pressure setpoint as a green line. Similarly, the left graph shows the same for voltage values, and the bottom graph shows current values. Optionally, the duty cycle toggle can be used to set the power supply limits to 0% after the elapsed time.

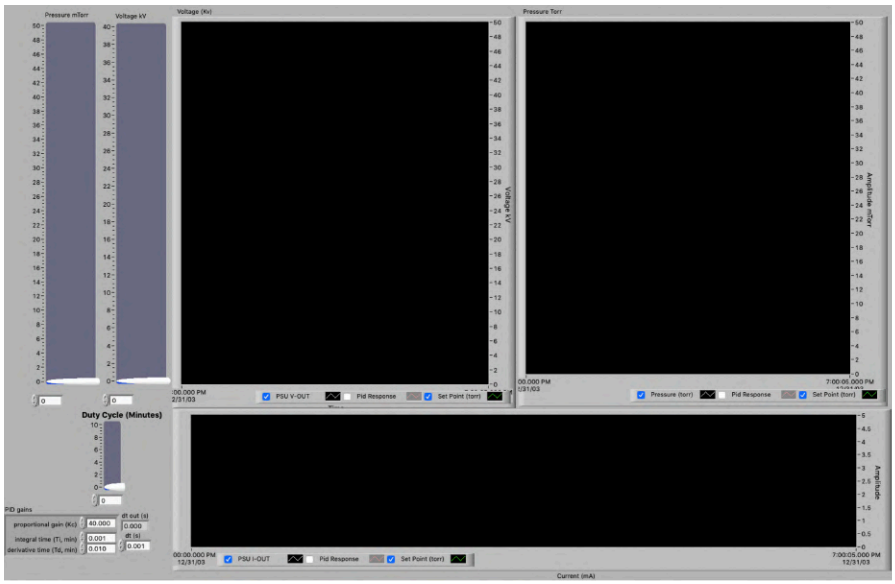

Figure 10. The front panel of the manual control tab from the LabVIEW VI used to control pressure.

4.1.5 The Neutron Detection System

In addition to pressure and voltage values, neutron flux was tracked. BTI PND fast neutron bubble dosimeters were selected because they are impervious to electric noise and x-ray or gamma background radiation, are delivered factory tested and calibrated, and have an isotropic angular response, i.e. they will record properly in all orientations. The uncertainty associated with the detectors from calibration and temperature response variations is +/- 20% [17]. The detectors are placed outside of the radiation shielding at fixed positions. Refer to the image and diagrams below for a visualization of their placement. The detectors outline in red are placed in different planes and are thus marked.

The BTI bubble detectors require the gel inside to be at room temperature to operate, and they respond to fast neutrons of the kind that the fusor emits. Recording neutron data from them requires counting the number of bubbles formed, the amount of time in which those bubbles formed, and the calibration sensitivity. The mounting locations were chosen because a test for neutron emission isotropy was desired. Because the radius can be factored out when back solving for neutron flux from the BTI detectors, distance can safely vary between positions as long as it is kept track of.

The only issue with the BTI detectors for this experiment is that they are prone to bubble formation via heating. As such they were be kept far enough away from the chamber to ensure they maintain room temperature. Even though this is the case, it is easily identifiable when the BTI detectors indicate counts due to heat, as the bubbles they form will be much smaller and closely packed than those from neutrons. The presence of such bubble clusters would indicate false counts and the need for a retrial.

The BTI detectors work in the following way according to their manufacturer. BTI notes, “Inside the detector, tiny droplets of superheated liquid are dispersed throughout a clear polymer. When a neutron strikes a droplet, the droplet immediately vaporizes, forming a visible gas bubble

trapped in the gel. The number of bubbles provides a direct measurement of the tissue-equivalent neutron dose."

Finally, detectors are placed in different positions around the radius of the device to allow for a test of isotropy. Because the geometry of the shielding enclosure, detectors were not placed at equidistant points away from the grid surface. Instead, they are placed as follows: detectors 1 and 6 are 28.7 cm away from the grid. Detectors 2, and 5 are 26.2 cm away. Detector 3 is 23.0 cm away from the grid. Detector 4 is 24.6 cm away from the grid.

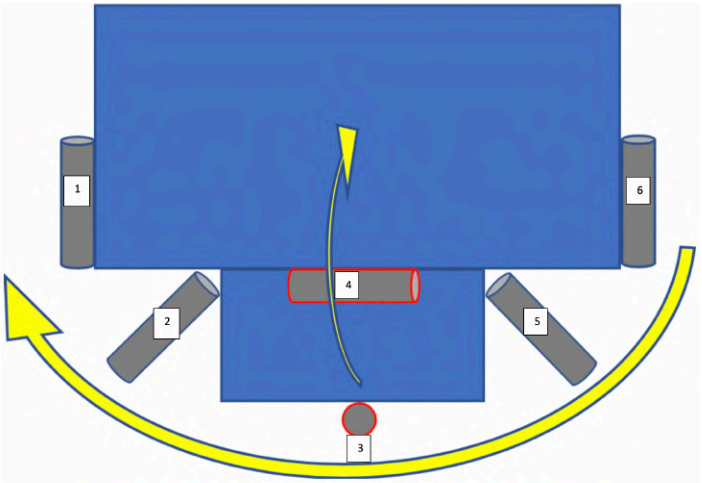

Figure 11. A figure depicting orientation, placement, and location number of each BTI detector as seen from a bird's eye view. The dimensions of the larger shielding box are as follows: 47.0 cm long, 25.5 cm wide, and 33.0 cm tall.

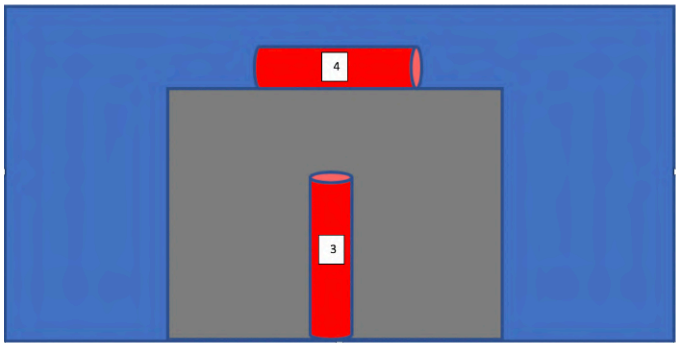

Figure 12. A figure depicting the front two bti detectors, shifted 90 degrees in perspective from the above figure. The blue surface represents the shielding that covers the main chamber, while the grey represents the removeable shielding piece that covers the viewport. The dimensions of the smaller shielding box are as follows: 30.5 cm long, 7.6 cm wide, and 25.4 cm tall.

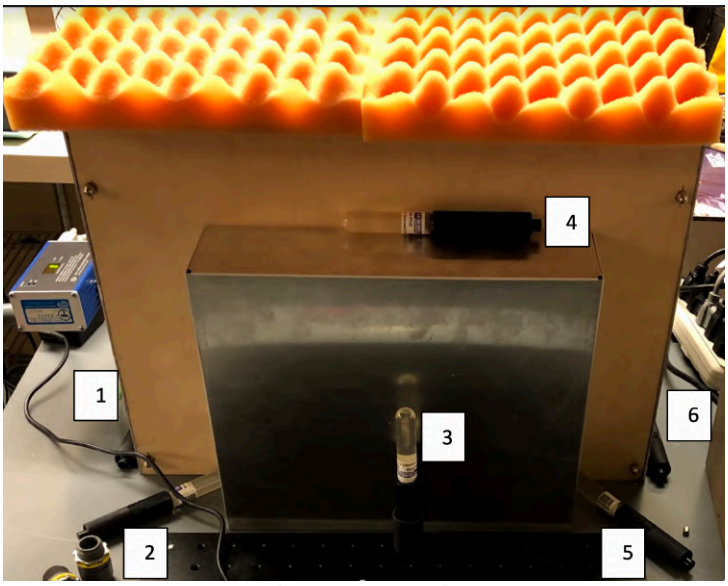

Figure 13. A photograph of the placement of each detector during a run.

4.1.5 The Ion Source

One of the goals of the work involves an attempt to increase ion concentration by mounting an ion source. This requires a few components to ensure that the ion source functions. First. 15V DC power is required, which is obtained from the I/O box of the machine. This feeds into an adjustable DC-DC converter that allows for 1.25 to 6 volt output. The ion source requires +4-6kV at a few mA to operate. To this end an EMCO F40 DC-DC converter was used to step up the 1.5-6Volt output of the regulator supply to the required +6kV or +4kV while under load. The ion source itself consists of an anode layer ion source designed by Technical Plasmas LLC. It is similar in nature to a hall thruster, which uses the hall effect and captured electrons to ionize the D2 atmosphere inside, but omits the neutralizer source on the exhaust as the goal is to generate ions not thrust. The ion source is mounted to a Lesker MHV feedthrough and power is fed via an MHV cable. Refer to the figure below for an overview of the ion source.

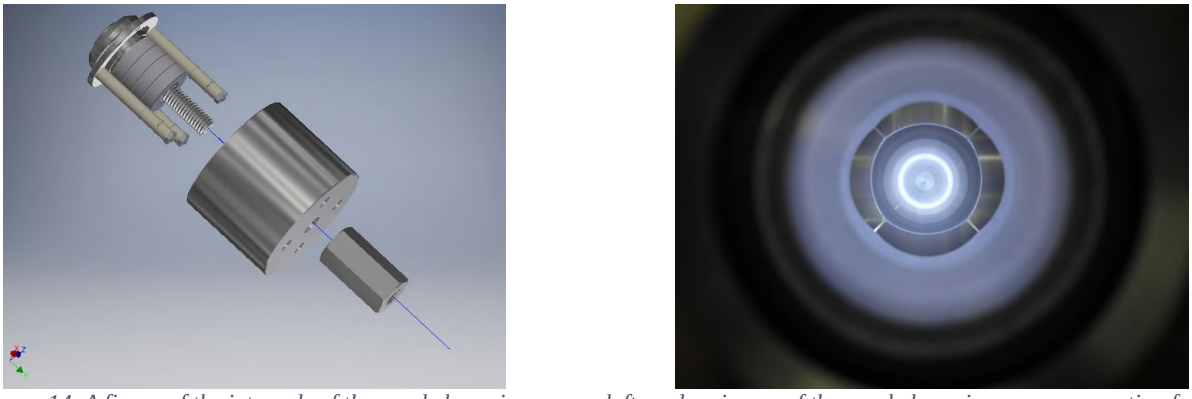
Figure 14. A figure of the internals of the anode layer ion source left, and an image of the anode layer ion source operating from [15]

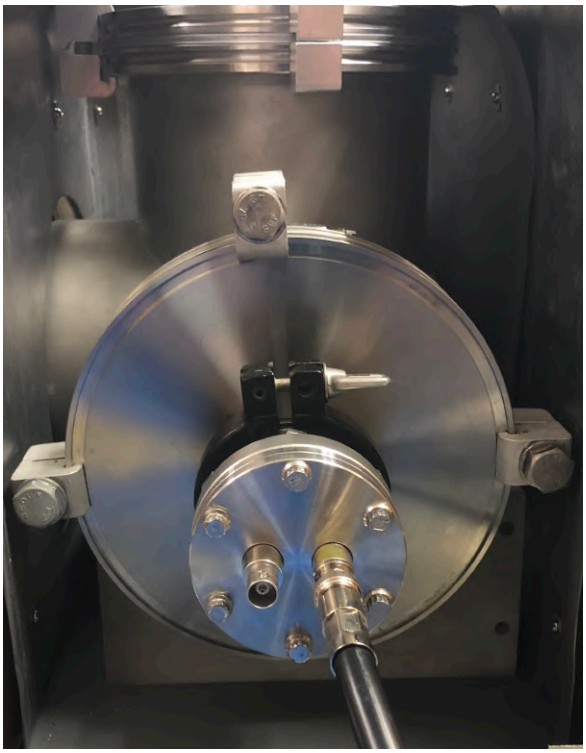

Figure 15. An image of the MHV feedthrough to which the ion source is mounted, installed and electrically connected.

4.2 Methods: Operation and Data Collection

4.2.1 Pre-Run Check

Before the device is operated, there are a few safety considerations. These are more clearly outlined in the proper order in the operations manual of the appendix, but the following must be checked. Because the fusor is essentially an electric circuit when a glow discharge is struck, there must be a return path. Thus, the ground connection must be properly checked to ensure that there is good electrical contact between the vacuum chamber or outer grid, and the ground line of the high voltage system. Next, pumps and connections must be checked to ensure there are no leaks in the vacuum line. Because the reaction rate strongly depends on fuel purity, a leak in any portion of the vacuum system can potentially have a substantial effect on fuel purity and this reaction rate. For this reason, it is advisable to have a residual gas analyzer to allow for monitoring of the fuel purity inside the chamber, and contaminants. Finally, it is important to ensure all high voltage connections are properly connected, as electrical noise caused by corona was found to be severe enough to shut down the control computer when long usb cables were connected. Such a loss of control could lead to extensive damage to the device and injury to the operator.

Once the pre-run checklist is complete, pumps are turned on and valves are opened in accordance to the operating manual. While the operator waits for the system to reach equilibrium, the detectors are made ready for use. The detectors work by forming bubbles in response to neutron capture. To ensure that the detectors may be used multiple times, there is a compression mechanism that is used to recompress the detection gel inside the detector to remove the bubbles.

This is done by screwing on the lid in the compression position. To ready the detector, the cap is removed, flipped around, and screwed back on. This is done to all detectors prior to turning on the power to the machine. While the fusor comes to full power, the detectors are kept far away from the device so that no neutrons are counted before the intended time frame.

4.2.2 Operation

Operation is detailed more completely in the operations manual in the appendix. Essentially the device is powered on entirely with the exception of the high voltage systems. Then pressure is set to a known safe value, and the system is given time to reach the pressure set point. A safe pressure value is defined as a pressure where the operator knows the system will operate stably. This is an ideal starting point because the system is more easily brought to full power by a slow and controlled pressure descent from this safe point, rather than brought to pull power from the start. This slow descent is also required because as plasma bombardment heats up the chamber walls, outgassing rate will massively increase, changing either the fuel pressure, composition, or both. This in turn will cause a change in allowed voltage for a particular pressure point, thus a slow descent through pressure values allows the system enough time to reach stable equilibrium with those outgassing changes.

For this particular system the deuterium pressure was around 9mTorr and the safe point around 12mTorr, i.e. at 12 mTorr the system would draw 5mA at -20kV or so while at 9mTorr, the system would be at full power, i.e. -40kV at 5mA. Once the maximum power is realized, the detectors are quickly brought to position and the timer is started. This timer is set for 10 minutes to allow for a balance between good counting statistics and lifetime of the components, as excessive heat is generated in the chamber, and large strain is placed on the power supply. To reduce systematic errors, the individual detectors are randomly placed in different detection spots each time.

4.2.3 Shutdown

Upon reaching the prescribed time for data collection, power is immediately cut from the device and the vacuum chamber is brought again to the safe pressure point for the next run. The operating manual in the appendix more completely details the procedure that was followed here. Once the run has concluded, the BTI detectors are reset using the mechanism described above in the operation section to be ready for the next run. Typical reset time for the new detectors is about 10 minutes from the point of compression, until all bubbles have disappeared. Additionally, the gas regulator was checked to ensure adequate fuel pressure was still being supplied to the mass flow controller (10-15PSI).

4.2.4 Note About Run Times

Run campaigns consisted of 5, 10-minute runs, and one 30-minute run depending on the experiment being conducted at the time. Run times were kept to 10 minutes to prevent long cool down times of equipment, to reduce sputtering of stainless-steel grid onto ceramic feedthroughs, and to limit the number of fuses that are consumed by the device. Unfortunately, in prior testing, it was found that continuous operation past 30 minutes would almost certainly result in a blown

fuse, even if replaced with 1amp higher capacity. 10-minute run times were well under this point, and thus suffered no such issues.

4.3 Methods: Experimental Procedure

4.3.1 Conditioning for Background Run Prior to Ion Source Installation

One key characteristic of vacuum plasma systems is that Paschen's law depends on gas composition. This means that any outgassing, impurities, or leaks will change the behavior and performance of the device. In addition to this, inner grids are built by hand as mentioned in section 4.1.2 which means that both oils from handling, and metal cracks, i.e. surface roughness will accumulate on the grid. Those oils will burn off contributing to outgassing, and the micro sharp points on the grid will be conditioned in a plasma discharge and be ablated off as operation occurs. Because these events draw high current, they buckle the supply and cause dips in voltages as the supply enters constant current mode. Similarly outgassing can cause pressure spikes and changes that will affect the power level in the same way. A system is taken to be conditioned when metal ablating events are no longer observed, and partial pressure of deuterium is stable for the entire duration of the operation. The second criteria is challenging to confirm in this device due to lack of a residual gas analyzer, but may be realized during the following way. First, consider that a pressure measurement alone is not a good indicator of deuterium partial pressure, as the PID controller will adjust fuel flow to keep pressure at the set point accordingly. Therefore, if slow outgassing occurs for example, the mass flow controller will slowly choke off deuterium flow to maintain the desired pressure, all the while deuterium partial pressure is decreasing at a rate beyond what is noticeable from the LabVIEW pressure display.

The most reliable indicator of deuterium partial pressure is as follows, suppose a 10-minute run is completed once plasma ablating events are over, and the run appears to have good stability as noted by constant pressure, voltage, and current values over the duration of the run. Once the run is over the dosimeter data and the pressure corresponding to the maximum supply power, should be logged. Then many runs in a similar fashion should be completed until the neutron flux measured at the same detector locations is constant, and until the value of the max power pressure remains unchanged. Then the system is taken to be conditioned and ready for data collection. This is not a state of perfect conditioning, i.e. a state where no leaks, outgassing, or any other impactful changes occur, rather, it is a state of stable equilibrium of those conditions, i.e. it is a state where for example outgassing rates will no longer change, and they have reached a small of value as possible for your system. Ultimately the consequence of this state is the desired outcome, which means that if neutron flux is constant for a constant set of operational parameters, then the system can be considered practically conditioned. Prior to the work outlined in this paper, the system underwent such conditioning for about a month. During this time, the walls of the chamber were assumed to be loaded with deuterium instead of water vapor, thus additional, inevitable, outgassing would ultimately be beneficial.

4.3.1.2 – Leak Testing

Another note about conditioning in this specific system is as follows, due to vibrations from the pumps, the Swagelok connections were able to vibrate loose in the gas lines. This meant that atmosphere was able to leak into the fuel lines. To check for this problem, and attempt to alleviate it, the following was done. First the system was pumped down to its baseline pressure, this value was the bottom of the convectron gauge (1mTorr). Then, the mass flow controller was set to fully open, 5 minutes were allowed to elapse, then the pressure was read. Initially, when the mass flow controller is opened, there will be a surge of pressure, as overnight leaks gradually backfill the fuel line from the chamber, and from the line fittings themselves. Because this rate is small, it is not of concern for the experiment, i.e. the experiment takes place on smaller orders of magnitude than the overnight leak rate. If after this initial accumulation of atmosphere in the fuel lines, pressure remains, and chamber pressure can thus rise past the system baseline, then a fast rate leak exists. If this is the case, the fittings were retightened with the mass flow controller fully open until the chamber pressure returned to zero. Again, this is important because the reaction rate strongly depends on fuel purity, and in prior work, it was found that even a 15PSI (atmosphere) leak had strong influence on the chamber fuel purity even if the deuterium feed pressure into the fuel line was 20 PSI (20 PSI being the upper limit of the regulator).

4.3.2 – Run Campaign 1 – Baseline Prior to Ion Source Installation

The IEC device was originally built to serve as a teaching tool and demo for classrooms as the Compact Classroom Fusion Device (CCFD). This combined with the fact that its performance had never before been benchmarked, meant that one the goals of the work was to characterize the baseline performance of the CCFD. To this end the first run campaign was done. This consisted of running the device for 5 runs of 10 minutes on different days to measure the neutron flux at different points around the device. Operation of the device was done in accordance with the operations manual and the sections described above, and pressure, voltage, current, and neutron data was logged. The run campaign was split up over a period of two weeks to ensure that operating conditions were more reflective of long-term system variations.

4.3.3 – Run Campaign 2 – Baseline After Ion Source Installation

Following the establishment of a baseline for the system with the first run campaign, the system's right port on the 5-way cross was opened up to allow for the mounting of an ion source. The ion source was assembled to the Lesker MHV feedthrough according to the instructions provided by Technical Plasmas LLC and the supporting power systems were assembled and tested to ensure that the ion source was receiving proper power. Because the ion source was handled and the system was opened up, two weeks or so of frequent conditioning runs took place to ensure that the system baseline performance, i.e. with the ion source turned off, would match the first run campaign. Then 5, 10-minute runs were taken in accordance to the device operating procedure outlined in the appendix. Pressure, voltage, current, and neutron data was collected and recorded.

4.3.4 – Run Campaign 3 – Pressure Dependence Test

Following the installation of the ion source, to verify that it was indeed working the ion source was set to the maximum power it would sustain and a single continuous 30-minute run was completed. Pressure, voltage, current, and neutron data was collected and recorded. This run was done to ensure that the ion source and new system would sustain continued run campaigns.

4.3.5 – Run Campaign 4 – Ion Source Turned on

Following the confirmation of stability from run campaign 3 the ion source was adjusted according to 7.3.1 and the final run campaign was completed. In this case, care was taken to ensure that max power pressure with the ion source was roughly the same as without (within 0.5mTorr) by running the ion source at the ideal power mentioned in 7.3.1.

5 Analysis Methods

5.1 Methods for Analyzing Input Parameters

Pressure, Voltage, Current, and ion source power are all inputs to the device. Together, and through Paschen's law the work to create specific operating conditions for the device. In this work, the operating region of interest was full power. This was the region where pressure was such that voltage, and current draw was maximized. To do this, pressure had to be maintained at 9mTorr (excluding campaign 3). Because pressure would always be driven to setpoint, the pressure value remained stable at the setpoint for the duration of the setpoint. In some cases, like campaign 3 the set point had to be adjusted down from 9mTorr to accommodate the pressure oscillations. In all cases, the live pressure was visually monitored on the LabVIEW VI front panel to check that there was no deviation from setpoint. Because LabVIEW shows the last 5 seconds of pressure data, the visual inspection only had to be completed in that interval.

Voltage strongly depended on pressure and was logged visually. Since pressure was stable for the duration of a run (excluding campaign 3), voltage was correspondingly stable. It was visually checked on the front panel of the high voltage power supply enclosure to ensure that no significant (greater than 200V) from 40kV occurred. If this occurred, pressure was correspondingly adjusted via the setpoint to maintain full voltage output from the supply.

Current was also visually inspected but was not at strongly tied to pressure as voltage was in campaign 4, with the ion source turned on. In this case, the current was constantly monitored and the ion source power was adjusted to force the supply to draw the full 5mA value.

5.2 Methods for Analyzing Output

The performance of the device was evaluated using a simple two parameter metric. Neutron emission, and stability of input parameters. Runs that were stable in terms of pressure, voltage, and current values were considered qualitatively to be of higher value than unstable runs. Neutron flux was calculated from a visual inspection of the bubble formation present in each BTI

detector. Section 4.1.5 details how the detectors capture neutrons at various rates according to their calibration. Once the 10 minutes of the run expired, the power was immediately turned off and detector data was logged. All detectors positions and orientations remained constant across all campaigns, but individual detectors were generally moved between positions from one run to another. This was done in an attempt to minimize error. The figure below shows a typical bubble formation after a neutron run.

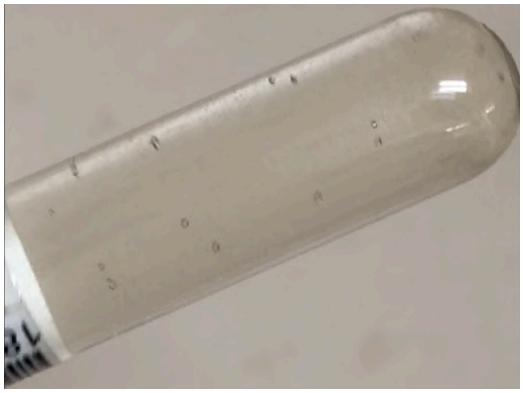

Figure 16. A photograph of a detector showing typical bubble production in a high neutron emission area. Run time shown is 10 minutes.

For each run, each of the 6 detectors had their bubbles counted, the calibration value of the detector was noted, and its position was noted. This was done for all detectors and for all runs. A timer was used to ensure that run duration was exactly 10 minutes.

5.4 Methods for Calculating Flux

To back out flux from the detectors a few key quantities are recorded. First, the amount of bubbles is recorded from each detector. The run time is known, as are the distances away from the surface of the grid. The calibration for each detector is also known. It is important to know that the detectors are intended to work as dosimeters, indicating with bubbles the tissue equivalent in absorbed dose. Thus, the first step is to calculate how many mRems of neutron radiation the detector has absorbed. To do this the following equation is used.

$$Dose\ Rate\ \left(\frac{mRem}{second}\right) = \frac{Number\ of\ Bubbles}{Time\ Elapsed\ (seconds) * Bubble\ Calibration\ Factor} \tag{1.6}$$

From here, the objective is to back out the number of neutrons that contribute to creating this dose. Using [18], for 2.45 MeV neutrons, this corresponds to a number of 28,000 neutrons per mRem. So now to convert the dose rate to a neutron flux at that location, the dose in mRem for the run time is multiplied by 28,000. Now that a given number of neutrons per unit time is calculated at that location, a sphere is considered whose surface area is defined by the radius (distance) from the detector location to the grid surface. The critical assumption here is that the grid surface is the origin of neutron emission. Using the above as the radius, $4\pi R^2$ gives the surface area of that sphere. Using the following equation, the total isotropic flux is calculated at that detector position using the above.

$$Isotropic\ Flux\ \left(\frac{neutrons}{second*cm^2}\right) = \ Dose\ Rate * 28000 * \ 4\pi R^2 \quad (1.7)$$

Where twice this value is the total reaction rate, or number of fusions, since only half of the deuterium – deuterium fusions yield a neutron, which can be measured, and the other half emit a proton which does not escape the vacuum chamber.

In the computation of error, a few assumptions, and idealizations were made. First, the detector forming bubbles is a binomial event i.e. either a bubble is formed or it isn't. For such a distribution the error the variance is modeled by the following equation.

$$\sigma^2 = \ \mathrm{np}(1 - \mathrm{p}) \quad (1.8)$$

where p is the probability of a bubble forming when a neutron passes into the detector, and np is the mean. Because p is very small and the same for all detectors standard deviation reduces to

$$\sigma = \ \sqrt{\mathrm{x}} \quad (1.9)$$

Where $\sqrt{x}$ is the standard error. For this reason, counting uncertainty is given as the above. Calibration uncertainty, as mentioned in section 4.1.5, is 20%. This is intrinsic to the BTI detectors due to the manufacturing process and cannot be improved. Measurement error is derived from the fact that various measurements of physical dimensions were taken with some error, and then they were used to compute a "crow's flight" distance from the grid. This too was computed using the standard rules for error propagation. Finally, a time error was included of 10 seconds for each run. Again, this was incorporated using the standard rules of error propagation. In the appendix, python code used to automate flux, total fusion amount, and error calculations is provided.

The procedure for computing flux values and associated errors was as follows. First the bubble count, detector calibration, time of run, and detector position was noted. These parameters were then input into the python script and a flux measurement with corresponding error was recorded. In the case where multiple flux values were averaged, their errors were processed according to the rules of error propagation. Wherever many such averages were computed, error was similarly propagated.

The values calculated are equivalent Isotropic Rates (N/S). Because the flux profile was not finely resolved, and because a 360-degree profile measurement was not done in this work, for simplicity, the calculated values below represent equivalent Isotropic Rates (N/S) with spheres that have the radius taken to be the distance from the detector to the grid surface. It is important to note that the flux is not in fact isotropic, instead emission favors detector positions 1 and 6 the most.

6 Data Summary

6.1 – Campaign 1

This run was very stable in terms of pressure and thus voltage and current draw from the fusor. During the period in which detectors were turned to the active state and placed in their corresponding locations, fuel pressure was turned as high as possible to allow for the high deuterium flow to flush out any possible lingering impurities. This run data was completed after roughly a month of conditioning, where runs were done at least twice every week during that month. Throughout the duration of the run, voltage and current levels were kept at full value, dipping rarely at most, 1kV and 0.1 mA below full power. Pressure was kept at around 9mTorr, and increased only 0.1 or 0.2 as each run went on to maintain maximum voltage and current levels. This increase likely results from the heating inside the chamber. Prior to starting the run, the system was checked for leaks, using the method described in section 4.3.1.2. At the 10-minute mark, power to the supply was shut, and pressure was set to the highest value possible. This was done for two reasons, a high flowrate would flush out any impurities that accumulated in the chamber (outgassing of chamber and viton surfaces, leaks, etc), which allows for the starting run conditions to be the same as the first run for the next one.

Table 1-1: Number of bubbles recorded, and calibration of corresponding BTI detector for campaign 1.

Campaign Number – Run Number	1 – 1	1 – 2	1 – 3	1 – 4	1 – 5
Amount of Bubbles at Detector 1- (Calibration)	**7** (21B/M)	**7** (21B/M)	**6** (21B/M)	**6** (23B/M)	**3** (23B/M)
Amount of Bubbles at Detector 2 - (Calibration)	**8** (23B/M)	**7** (22B/M)	**2** (21B/M)	**6** (21B/M)	**5** (21B/M)
Amount of Bubbles at Detector 3 - (Calibration)	**5** (21B/M)	**7** (23B/M)	**2** (21B/M)	**2** (21B/M)	**2** (23B/M)
Amount of Bubbles at Detector 4 - (Calibration)	**5** (22B/M)	**8** (23B/M)	**8** (23B/M)	**3** (23B/M)	**4** (21B/M)
Amount of Bubbles at Detector 5 - (Calibration)	**1** (21B/M)	**4** (21B/M)	**10** (23B/M)	**3** (21B/M)	**0** (21B/M)
Amount of Bubbles at Detector 6 - (Calibration)	**6** (23B/M)	**10** (21B/M)	**2** (22B/M)	**3** (22B/M)	**5** (22B/M)
Total Amount of Bubbles	**32**	**43**	**30**	**23**	**19**

6.2 – Campaign 2

The run initially had some small voltage / current instabilities, where the voltage and current values would drop from max power. At most these departures from full power values were 2kV and 1mA for less than 2 seconds, as such they were not deemed significant and the run was completed. Pressure remained constant at 9mTorr throughout the run, only increasing by a small amount 0.1, 0.2 as the run went on, as in the previous run. Typically, voltage and current fluctuations indicate that conditioning is not complete, as this instability results from outgassing and in this case, plasma conditioning events events on the grid. This run data was completed after roughly two weeks of conditioning, where runs were done at least twice every week during that two-week period. The system was opened to atmosphere between campaign 1 and 2, and some surfaces were handled with a bare hand. This coupled with the fact that conditioning was only done for two weeks instead of four for this run campaign, meant that the system still displayed some minor stability fluctuations. During the period in which detectors were turned to the active state and placed in their corresponding locations, fuel pressure was turned as high as possible to allow for the high deuterium flow to flush out any possible lingering impurities. Prior to starting the run, the system was checked for leaks, using the method described in section 4.3.1.2. At the 10-minute mark, power to the supply was shut, and pressure was set to the highest value possible.

Table 1-2: Number of bubbles recorded, and calibration of corresponding BTI detector for campaign 2.

Campaign Number – Run Number	2 – 1	2 – 2	2 – 3	2 – 4	2 – 5
Amount of Bubbles at Detector 1- (Calibration)	**5** (23B/M)	**4** (22B/M)	**6** (22B/M)	**4** (22B/M)	**6** (22B/M)
Amount of Bubbles at Detector 2 - (Calibration)	**2** (21B/M)	**5** (21B/M)	**8** (21B/M)	**6** (21B/M)	**3** (21B/M)
Amount of Bubbles at Detector 3 - (Calibration)	**3** (23B/M)	**4** (21B/M)	**3** (21B/M)	**3** (21B/M)	**5** (21B/M)
Amount of Bubbles at Detector 4 - (Calibration)	**4** (21B/M)	**5** (21B/M)	**11**(21B/M)	**5** (21B/M)	**8** (21B/M)
Amount of Bubbles at Detector 5 - (Calibration)	**3** (21B/M)	**4** (23B/M)	**0** (23B/M)	**2** (23B/M)	**2** (23B/M)
Amount of Bubbles at Detector 6 - (Calibration)	**4** (22B/M)	**4** (23B/M)	**8** (23B/M)	**7** (23B/M)	**5** (23B/M)
Total Amount of Bubbles	**21**	**26**	**36**	**27**	**29**

6.3 – Campaign 3 (1, 30-minute run)

This first iteration of this campaign was initially unstable, as the ion beam created by the source was aimed into the convectron sensor. Even though the convectron sensor has a fine grounded mesh on its input, this was not enough to stop ion bombardment of the sensor and thus cause +/2mTorr pressure oscillations. To better cope with this issue, the original campaign 3 data was discarded and a new campaign was started where a previously mounted gauge was used for pressure sensing instead. This other gauge was a similar distance away from the grid, across from the fuel input port, but because the entire chamber was in molecular flow, the pressure reported by this sensor would have been the same in the upper section of the chamber, near the previous grid. For this reason, no changes were made to run setup. With the new grid placement, the run was stable, but pressure was around 5mTorr because the ion source was turned up to full power. Section 7.3.1 explains the effects of using an improperly tuned ion source power in this manner. Once the 30-minute run time was complete, the campaign was concluded and the system power was cut, and the device was completely powered off. This campaign consisted of one long run because it was done as a stress test of a system, to demonstrate whether the ion source installation was successful. Inadvertently, it also functioned as an experiment to demonstrate system behavior with an ion source mounted and with improper power settings.

Table 1-3: Number of bubbles recorded, and calibration of corresponding BTI detector for campaign 3.

Campaign Number – Run Number	3 – 1
Amount of Bubbles at Detector 1 (23B/M)	4
Amount of Bubbles at Detector 2 (21B/M)	3
Amount of Bubbles at Detector 3 (21B/M)	3
Amount of Bubbles at Detector 4 (22B/M)	9
Amount of Bubbles at Detector 5 (21B/M)	4
Amount of Bubbles at Detector 6 (23B/M)	6
Total Amount of Bubbles	29

6.4 – Campaign 4

This run was very stable in terms of pressure and thus voltage and current draw from the fusor. During the period in which detectors were turned to the active state and placed in their corresponding locations, fuel pressure was turned as high as possible to allow for the high deuterium flow to flush out any possible lingering impurities. This run data was completed after campaigns 2 and 3, which was equivalent to about the same conditioning levels that campaign 1 started out with. Throughout the duration of the run, voltage and current levels were kept at full value, dipping rarely at most, 1kV and 0.1 mA below full power. Pressure was kept at around 9mTorr, and increased only 0.1 or 0.2 as each run went on to maintain maximum voltage and

current levels. This increase likely results from the heating inside the chamber. Prior to starting the run, the system was checked for leaks, using the method described in section 4.3.1.2. At the 10-minute mark, power to the supply was shut, and pressure was set to the highest value possible.

Table 1-4: Number of bubbles recorded, and calibration of corresponding BTI detector for campaign 4.

Campaign Number – Run Number	4 – 1	4 – 2	4 – 3	4 – 4	4 – 5
Amount of Bubbles at Detector 1- (Calibration)	**4** (21B/M)	**10** (21B/M)	**9** (22B/M)	**8** (23B/M)	**11** (21B/M)
Amount of Bubbles at Detector 2 - (Calibration)	**1** (23B/M)	**0** (22B/M)	**2** (23B/M)	**1** (23B/M)	**1** (23B/M)
Amount of Bubbles at Detector 3 - (Calibration)	**2** (21B/M)	**3** (21B/M)	**5** (21B/M)	**5** (21B/M)	**6** (21B/M)
Amount of Bubbles at Detector 4 - (Calibration)	**6** (21B/M)	**6** (21B/M)	**4** (23B/M)	**6** (21B/M)	**8** (23B/M)
Amount of Bubbles at Detector 5 - (Calibration)	**6** (22B/M)	**1** (23B/M)	**3** (21B/M)	**0** (22B/M)	**2** (21B/M)
Amount of Bubbles at Detector 6 - (Calibration)	**6** (23B/M)	**11** (23B/M)	**11** (21B/M)	**7** (21B/M)	**8** (22B/M)
Total Amount of Bubbles	**25**	**31**	**34**	**27**	**36**

7 Results and Discussion

7.1 Campaign 1 Results and Discussion

This campaign was particularly valuable because it was done after roughly a month of conditioning. The flux numbers obtained taken to be baselines as pressure voltage and current values were all very stable of the course of the runs. Even without the ion source mounted, there is a vague anisotropic shape in the neutron emission of the device. When all runs in the campaign are taken in average at each detector position, the anisotropy strongly favors the detector 1 and 6 positions. It is also important to note that there is an increase beyond the error region in flux from detector 3 to 4, suggesting 3-dimensional anisotropy in the base device. Section 7.5 will cover the general notion as to why this might happen, but because there are so many variables interacting in this machine, it is hard to pin down the cause on one particular variable without extensive further work.

Table 2-1: Flux calculation with error and corresponding detector calibration for campaign 1.

Campaign Number – Run Number	1 – 1	1 – 2	1 – 3	1 – 4	1 – 5
Flux at Detector 1 - (Calibration)	**161,012** ± **58,949** (21B/M)	**161,012** ± **58,949** (21B/M)	**138,010** ± **52,799** (21B/M)	**126,010** ± **48,208** (23B/M)	**63,005** ± **29,135** (23B/M)
Flux at Detector 2 - (Calibration)	**140,017** ± **49,348** (23B/M)	**128,084** ± **46,893** (22B/M)	**38,338** ± **19,536** (21B/M)	**115,014** ± **44,001** (21B/M)	**95,845** ± **38,611** (21B/M)
Flux at Detector 3 - (Calibration)	**73,862** ± **29,756** (21B/M)	**94,415** ± **34,566** (23B/M)	**29,544** ± **15,056** (21B/M)	**29,545** ± **15,056** (21B/M)	**26,976** ± **13,746** (23B/M)
Flux at Detector 4 - (Calibration)	**80,655** ± **32,492** (22B/M)	**123,438** ± **43,505** (23B/M)	**123,438** ± **43,505** (23B/M)	**46,289** ± **21,405** (23B/M)	**67,597** ± **28,969** (21B/M)
Flux at Detector 5 - (Calibration)	**19,169** ± **11,139** (21B/M)	**76,676** ± **32,860** (21B/M)	**175,021** ± **57,927** (23B/M)	**57,507** ± **26,592** (21B/M)	**0** ± **0** (21B/M)
Flux at Detector 6 - (Calibration)	**126,010** ± **48,208** (23B/M)	**230,017** ± **76,130** (21B/M)	**43,912** ± **22,377** (22B/M)	**65,869** ± **30,459** (22B/M)	**109,781** ± **44,225** (22B/M)

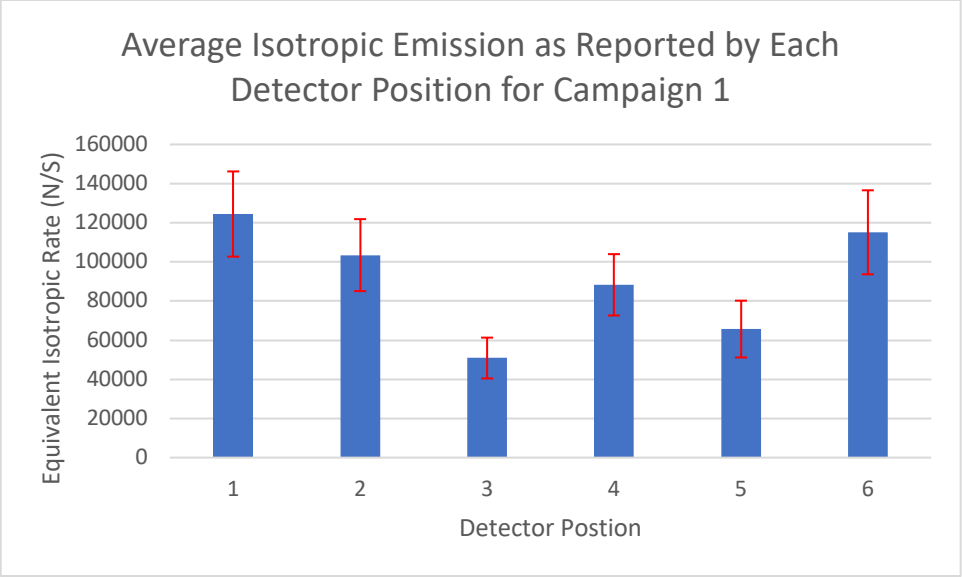

Figure 17. A graphical representation of the flux values with corresponding error averaged over all runs in the campaign, given according to detector position for campaign 1.

7.2 Campaign 2 Results and Discussion

Campaign 2 was completed after the system was opened to air and the ion source was installed. As mentioned previously, this run was preceded by conditioning runs, but they were not at extensive as the conditioning runs that preceded campaign 1. The new baseline of the machine was taken, and total bubble counts across all runs is approximately the same (with about 5%). This suggests that additional conditioning was not required, especially given that this campaign exhibited the same stability as campaign 1. For this particular run, the anisotropy identified in campaign 1 wasn't the same. Instead, neutron emission more strongly favored the middle detectors (3 and 4). Because this change wasn't very large, it's difficult to attribute it to anything to the exclusion of random error. Again, more work with better counting statistics, with a different detector system would answer the question of whether the flux difference is attributable to noise, or some detector error.

Table 2-2: Flux calculation with error and corresponding detector calibration for campaign 2.

Campaign Number – Run Number	2 – 1	2 – 2	2 – 3	2 – 4	2 – 5
Flux at Detector 1 - (Calibration)	**105,008 ± 42,302** (23B/M)	**87,825 ± 37,637** (22B/M)	**131,737 ± 50,400** (22B/M)	**87,825 ± 37,637** (22B/M)	**131,737 ± 50,400** (22B/M)
Flux at Detector 2 - (Calibration)	**38,338 ± 19,536** (21B/M)	**95,845 ± 38,611** (21B/M)	**153,352 ± 54,048** (21B/M)	**115,014 ± 44,002** (21B/M)	**57,507 ± 26,592** (21B/M)
Flux at Detector 3 - (Calibration)	**40,464 ± 18,711** (23B/M)	**59,090 ± 25,323** (21B/M)	**44,317 ± 20,493** (21B/M)	**44,317 ± 20,493** (21B/M)	**73,862 ± 29,756** (21B/M)
Flux at Detector 4 - (Calibration)	**67,597 ± 28,968** (21B/M)	**84,496 ± 34,039** (21B/M)	**185,892 ± 59,925** (21B/M)	**84,496 ± 34,039** (21B/M)	**135,194 ± 47,648** (21B/M)
Flux at Detector 5 - (Calibration)	**57,507 ± 26,592** (21B/M)	**70,008 ± 30,002** (23B/M)	**0 ± 0** (23B/M)	**35,004 ± 17,838** (23B/M)	**35,004 ± 17,838** (23B/M)
Flux at Detector 6 - (Calibration)	**87,825 ± 37,637** (22B/M)	**84,006 ± 36,001** (23B/M)	**168,013 ± 59,215** (23B/M)	**147,011 ± 53,823** (23B/M)	**105,008 ± 42,302** (23B/M)

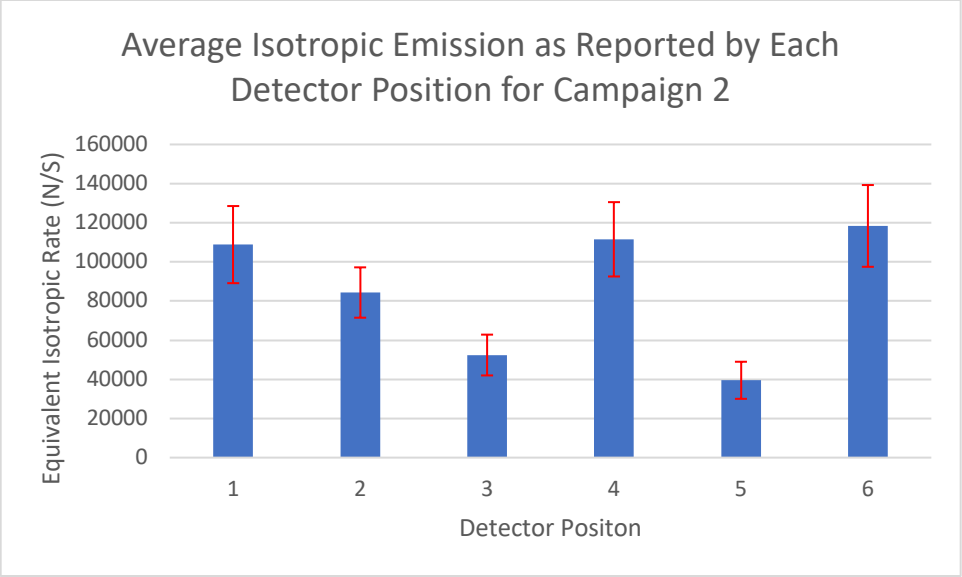

Figure 18. A graphical representation of the flux values with corresponding error averaged over all runs in the campaign, given according to detector position for campaign 2.

7.3 Campaign 3 Results and Discussion

Campaign 3 displayed various pressure and thus voltage and current fluctuations as mentioned previously. It was still a valuable run for the reason that it revealed an unexpected interaction between the ion source and the power supply in this system. Because the ion source power was set improperly during this campaign, neutron flux was a lot lower. Section 7.3.1 explains the source of this decrease in flux. While the run wasn't valuable in terms of further providing a baseline of the system, it was successful in characterizing the relation between the ion source and the power supply on this particular system.

7.3.1 – Ion Source / Power Supply Interaction

There is a key interaction between the ion source and power supply that must be noted and understood, as it serves to dictate how operating variables should be set when running with the ion source. First, consider why the fusor draws current, due to field emission, ion collisions with the grid, thermionic emission, etc electrons are lost from the main grid and usually taken to ground, or pumped out in the case of electron ion recombination to form neutrals. This loss of electron requires current to replace, and the rate of electron loss is proportional to voltage, i.e. the higher voltage grows, the more current is demanded from the supply to sustain the glow discharge, i.e. create new ions. It's also proportional to pressure, i.e. the number of ions that can be created, and thus the amount of current drawn varies with pressure, i.e. the higher the pressure, the more current is required to sustain a glow discharge.

At some pressure point, depending on the parameters in Paschen's law, the system will draw the maximum power output of the supply, suppose this is called the max power pressure. If the ion source is left off, and a system at max power pressure has its pressure decreased, because the amount of ionization that occurs is proportional to pressure, and because the supply is voltage and current limited, the pressure decrease will serve to starve the machine of ions and stop the

glow discharge. This pressure is achieved by setting the system to max power pressure, then slowly turning down the pressure in 0.1 mTorr increments until current draw of the high voltage power supply reads 0mA and voltage still reads a full -40kV. This is the point just below the Paschen minimum, i.e. the point just below where the system is able to provide the minimum amount of voltage and current to sustain a glow discharge, suppose we call this point the minimum pressure.

It is at minimum pressure that the ion source must be just turned on at the lowest setting. Once the ion source is on, there will be some current draw on the supply because the ion source is now supplying the ions that the grid cannot. The power to the ion source from here is gradually turned up only until the high voltage power supply reads maximum current draw (5mA) again. This is considered to be a properly tuned power level for the ion source. The max power pressure in this case should be very close to the max power pressure without the ion source. There is a danger of turning the power up to the ion source past this point. If the ion source is turned up past this point, (suppose it's called ideal ion source power), then the ions will overwhelm the power supply, in that more current draw will be required to cope with the amount of electron depletion that more ions result in. Because the supply can only provide a maximum of 5mA, anything past this point causes the supply to go into constant current mode.

This is a mode where the supply essentially reduces its voltage to ensure that it does not go over its current limit. As mentioned above however, there would seem to be a solution to this, but as will be explained, this solution is very undesirable. Because the number of ions depends on pressure and voltage, if the supply is at the constant current mode, then a decrease in pressure will cause a decrease in ion population, which will in turn allow the voltage to rise again, and thus the ion population again. The more power the ion source has, i.e. the more it pushes the high voltage power supply into the constant current regime, the larger the pressure drop will have to be to allow the power supply to operate at max power (-40kV at 5mA). The problem with this solution is that the system now ends up at a much lower fuel pressure, while at max power, and because reaction rate strongly depends on deuterium pressure, neutron flux strongly decreases, even though the system appears to be running at peak power.

There are a few concepts to note here, first this implies that increasing fuel purity, and fuel pressure is not only desired at maximum power, but that up to a point, higher fuel purity and pressure can be sustained at max power, suggesting that max power pressure isn't a static quantity that only depends on parameters from Paschen's law, rather it depends in part on the amount of ions present in the system. For a given equilibrium quantity of ions X, the system can sustain a max voltage and current Y, either percent ionization can increase, which mandates a decrease in pressure to conserve X, or percentage ionization can decrease, which mandates that pressure much increase to conserve X. Because Y can be had at all levels X within some range, the X corresponding to highest fuel pressure and purity, i.e. lowest percent ionization should yield the maximum neutron flux.

This was not apparent prior to the analysis of the data from run campaign 3, so run campaign 4 continued. This was not of excessive concern for run campaign 4 because the ideal ion source power meant that pressure would be close to the baseline cases. Further, another realization is that ion sources are useful for situations where excessive current draw is required from the

system. The addition of more / bigger / more efficient ion sources would result in increased ion number and thus additional current draw. Finally, because the voltage and current draw of the machine depends on the power level of the ion source, it is more desirable to run a system at the ideal ion source power, and control the ion source power level within a small margin as a way to set main system power without depending on the pressure mechanism which for industrial machines would suffer from great hysteresis.

Table 2-3: Flux calculation with error and corresponding detector calibration for campaign 3.

Campaign Number – Run Number	3 – 1
Flux at Detector 1 - (Calibration)	**28,002** ± **12,000** (23B/M)
Flux at Detector 2 - (Calibration)	**19,169** ± **8,864** (21B/M)
Flux at Detector 3 - (Calibration)	**14,772** ± **6,831** (21B/M)
Flux at Detector 4 - (Calibration)	**48,393** ± **16,496** (22B/M)
Flux at Detector 5 - (Calibration)	**25,559** ± **10,953** (21B/M)
Flux at Detector 6 - (Calibration)	**42,003** ± **16,069** (23B/M)

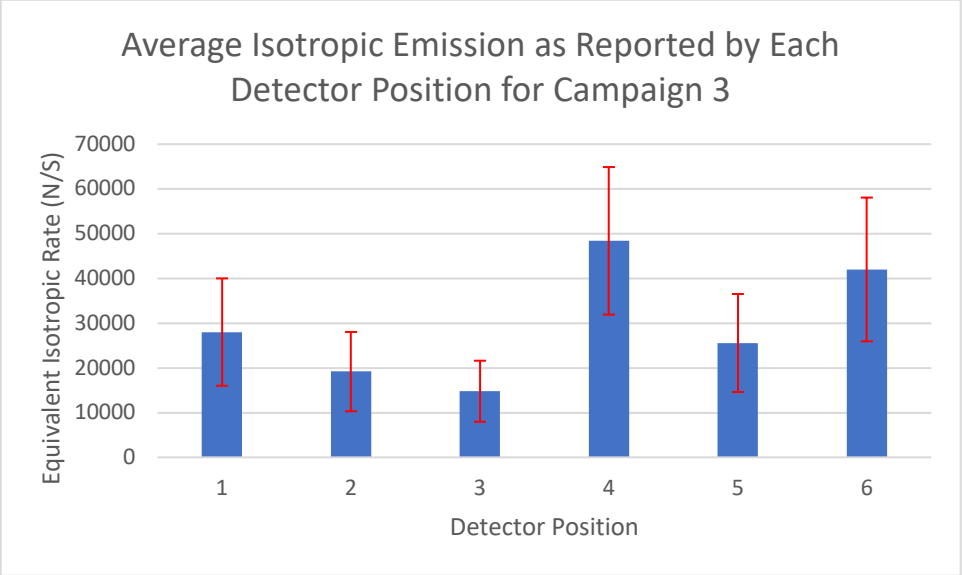

Figure 19. A graphical representation of the flux values with corresponding error averaged over all runs in the campaign, given according to detector position for campaign 3.

7.4 Campaign 4 Results and Discussion

Campaign 4 is particularly surprising as it appears that the effect of the ion source wasn't to increase flux overall, rather it was to exaggerate the initially observed emission anisotropy. This likely has happened because a large number of ions were concentrated along the direction of the ion beam, which was mounted in the largest free path, i.e. the path with the most amount of chamber space available to ions. The following should be noted about mean free path and recirculation in the fusor, in principle, an ion that starts at the left most edge can only recirculate to come to that same point, thus avoiding a collision with the wall. But if it collides with a neutral or another ion, or becomes a neutral on its recirculation path, then it's possible for the ion to collide with the wall. For this reason, the largest effective free path is the path where the

chamber wall to grid distance is greater than the mean free path. The neutron emission along this path (left port to right port) was, as mentioned above, already higher than other areas, so whatever distortion was present before, was amplified because now more ions participated in that distortion. Again, without more data, better counting statistics, different counting setups, its impossible to rule out error or noise of some kind, but that is beyond the scope of this paper. As measured with the BTI detectors, turning on the ion source has a consistent and noticeable effect of shifting the neutron emission to the left and right ports of the cross.

Table 2-4: Flux calculation with error and corresponding detector calibration for campaign 4.

Campaign Number – Run Number	4 – 1	4 – 2	4 – 3	4 – 4	4 – 5
Flux at Detector 1 - (Calibration)	**92,007 ± 39,430** (21B/M)	**230,018 ± 76,130** (21B/M)	**207,016 ± 70,569** (22B/M)	**84,006 ± 36,001** (23B/M)	**253,019 ± 81,565** (21B/M)
Flux at Detector 2 - (Calibration)	**17,502 ± 10,170** (23B/M)	**0 ± 0** (22B/M)	**38,338 ± 19,536** (23B/M)	**17,502 ± 10,171** (23B/M)	**17,502 ± 10,171** (23B/M)
Flux at Detector 3 - (Calibration)	**29,545 ± 15,056** (21B/M)	**44,317 ± 20,493** (21B/M)	**73,862 ± 29,756** (21B/M)	**73,862 ± 29,756** (21B/M)	**88,635 ± 33,910** (21B/M)
Flux at Detector 4 - (Calibration)	**101,395 ± 38,792** (21B/M)	**101,395 ± 38,792** (21B/M)	**61,719 ± 26,450** (23B/M)	**101,396 ± 38,791** (21B/M)	**123,438 ± 43,505** (23B/M)
Flux at Detector 5 - (Calibration)	**109,786 ± 42,002** (22B/M)	**17,502 ± 10,171** (23B/M)	**57,507 ± 26,592** (21B/M)	**0 ± 0** (22B/M)	**38,338 ± 19,536** (21B/M)
Flux at Detector 6 - (Calibration)	**126,010 ± 48,208** (23B/M)	**231,018 ± 74,472** (23B/M)	**253,019 ± 81,565** (21B/M)	**161,012 ± 58,949** (21B/M)	**175,650 ± 61,907** (22B/M)

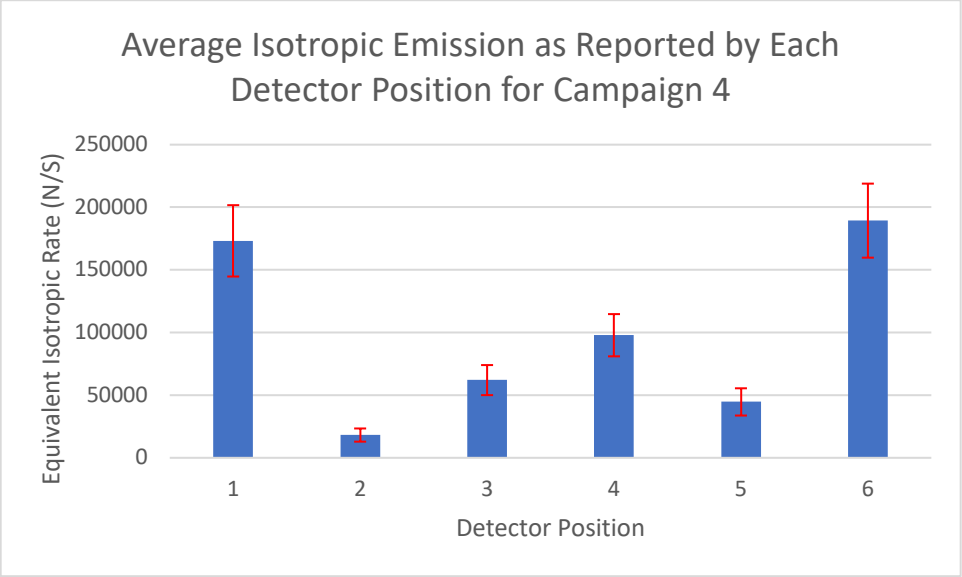

Figure 20. A graphical representation of the flux values with corresponding error averaged over all runs in the campaign, given according to detector position for campaign 4.

7.5 Overall Results and Discussion

It is worthy of noting that the device, even without the ion source mounted, shows a flux shape that is not isotropic. There are a few things to note about the shape of the profile as presented. Detectors 1 and 6 are on the outer edges and provide a larger flux reading than the detectors in the corners i.e. detectors 2 and 5. Detector 3 also shows a flux dip, but detector 4 shows a flux increase. Because of the large uncertainty associated with this counting setup, it is hard to tell whether there is a lack of isotropy in the direction going from detector 3 to 4, but anisotropy appears even past the uncertainty for the outer edges. This shape is possibly due to a larger mean

free path being available in the arms of the cross. From [2], the mean free path of ions in the system is less than device diameter. This mean free path gets quickly cut off in any direction that isn't in line from one cross to another. From the left port to the right port on the cross, the largest path is available for ions, and correspondingly the largest flux is seen there. The path from the viewport to the back of the cross is the smallest path available to ions excluding the small corner regions where the cross is welded. Accordingly, the smallest flux is seen here.

It is also important to note that the grid openings were oriented such that the "star mode" electron beams were along both the left to right port path, and the viewport to grid path. This likely did not contribute to changing the flux shape because while both detector pairs 3 and 4, and 1 and 6 had the grid opening in their direction, flux shape differed the largest between these measurement points.

To summarize the impact of the ion source, the figure below was created by taking an average of fluxes as measured at each detector from campaigns 1 and 2, marked by blue squares, and then compared to the flux average as indicated by detector position for campaign 4, i.e. the campaign with the ion source turned on.

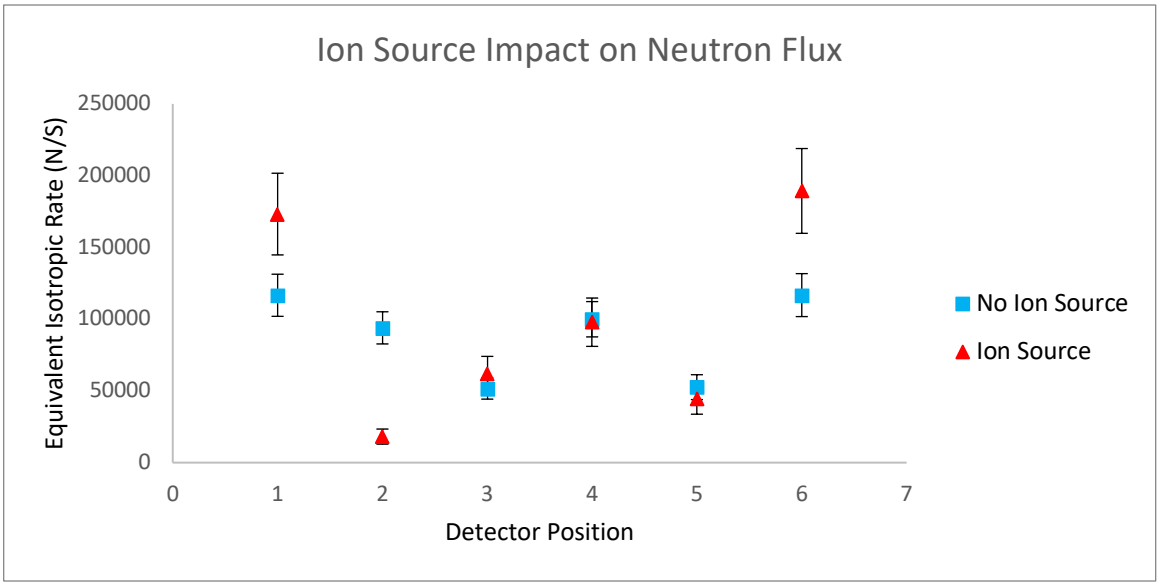

Figure 21. Impact of ion source on flux. Figure shows a comparison of campaign 4 to the averages of campaigns 1 and 2.

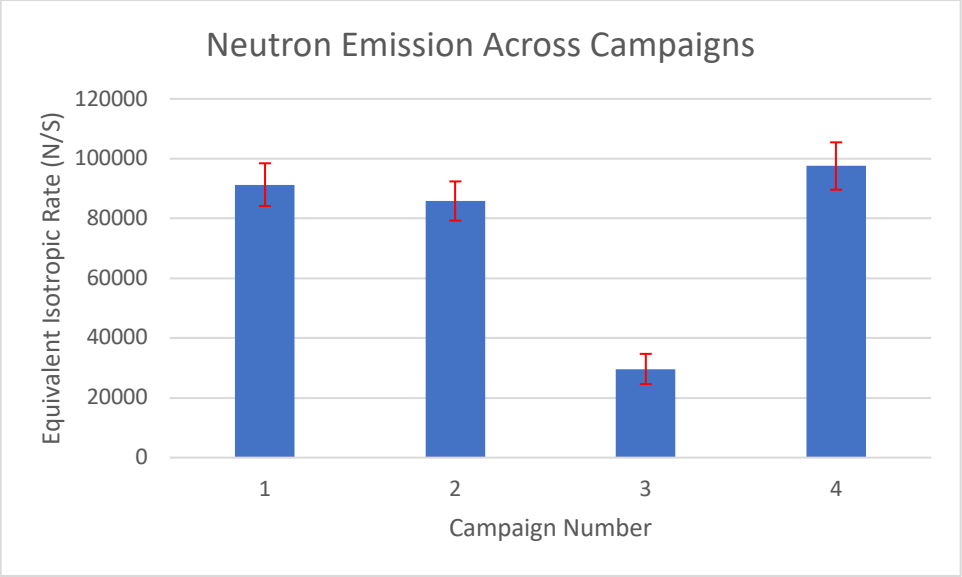

Figure 22. A graphical representation of the overall neutron emission across each campaign.

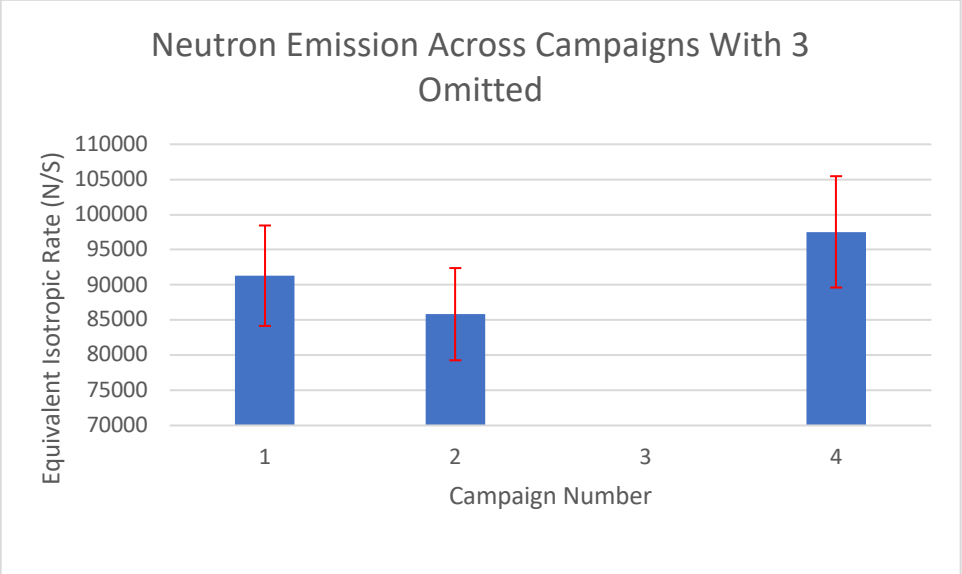

Figure 23. A graphical representation of the neutron emission across each campaign with campaign 3 omitted via axis rescaling for better comparison between ion source off and on campaigns.

8. Conclusion

In addition to what appear as marginal improvements in the overall neutron emission of the CCFD, the main effect that operation with an ion source had on the system was to push the flux profile towards the left and right ports. Flux at detectors 1 and 6 greatly increased compared to the baseline runs, while flux at detectors 2 and 5 greatly decreased. Flux at detectors 3 and 4 remained the same in both ion and no ion source runs. This effect was very consistent, and more noticeable with the ion source turned on.

Because the counting statistics were so poor, and the intrinsic errors of the detectors was so large, further work has to be done to determine whether a statistically significant increase of flux can be had from use of ion source in the CCFD. The use of alternate detectors, and alternate counting methods, alongside with more measurement channels would not only help to remove systematic error, but also offer better resolution of the flux shape.

In addition to the objective discussed above, the baseline of the CCFD was characterized. Running at 40kV with 5mA is possible at a pressure of 9mTorr, and will yield about 100,000 neutrons per second "isotropic" emission at the hottest points (detector positions 1 and 6). In these positions 8 or more bubbles is a common occurrence over a 10-minute run, making it ideal for a live demonstration of nuclear fusion with a portable IEC device. It is also of value that the system is able to maintain stable and safe operation at this level with the current automated pressure control scheme and lead shielding.

In addition, an ion source is deemed beneficial as a means of being able to rapidly control current draw, and thus reaction rate when operating with the ion source properly tuned as described in 7.3.1. This allows for more dynamic and faster control of the plasma than relying on pressure and Paschen's law, which is much slower to act as the system (hysteresis) grows larger.

9 Future Work

9.1 – Device Modifications

For future work, the device will have to be modified in a few ways to allow for monitoring of additional operational parameters, and for the improvement of operational capabilities. First an RGA mounted to the tank to allow for monitoring of fuel conditions inside the chamber allows for more consistent run to run performance, and allows the user to start a run only when proper fuel purity is met. Further, an RGA may be used to identity leaks, oil back streaming, and outgassing either naturally occurring or due to plasma bombardment. Finally, advanced RGA's are able to measure live cross sections for various interactions, like charge exchange in real time in the device. A more advanced RGA like this would allow for direct measurement of the percentage ionization of the fuel in the chamber, and would the direct measurement of the effect that change in the ion concentration would have on the charge exchange cross section and the reaction rate. In this paper, such effects were inferred to have occurred from neutron data alone, but given how many operational variables interact, it's hard to say whether random differences in plasma conditions, a different effect, or error / noise created the measured increase in neutron flux with the ion source.

A larger power supply capable of higher voltages, currents to allow a broader sweep of possible operational ranges would be useful for further characterizing the behavior pointed out in 7.3.1 – Ion Source / Power Supply Interaction. To support such a supply thermally, a liquid cooled grid like that described in [14] would be required to prevent melting of the grid at high input power, and would serve to reduce wasted power by reducing thermionic emission. Similarly, the main chamber would have to be cooled to protect electronics and KF seals. Ideally all gasketed areas

would be primarily cooled. More often helium leak detection would ideally occur as well as more frequent bake-outs, to identify and remove potentially problematic leaks.

9.2 – Different Studies

As implied by section 7.3.1 – Ion Source / Power Supply Interaction, the experiment carried out in run campaign 3, suggests that a system with minimum percent ionization and maximum fuel pressure and purity would yield the highest reaction rate, but there was an increase in average count rate for campaign 4 i.e. with the ion source turned on, in comparison to any other run campaign. Because it's possible that the results in run campaign 4 were caused by some other mechanics, experimental error, random error / noise, a more thorough investigation should be conducted in the manner outlined in 7.3.1, with broader sweeps of ion source power, ion source number, and pressure as allowed by a bigger supply and a cooled system. During such a study an advanced RGA like the one mentioned above that would allow direct measurement of cross sections of interest would be particularly useful.

As mentioned above, a large sweep of operational values would be valuable as they could potentially reveal a new operational mode, a new mechanism that may benefit IEC operation, or a change in operational characteristics. To this end a more detailed study of the isotropy assumption of the neutron emission of device, as it relates to grid and chamber geometry, or any other parameters would be useful in further revealing possible ways in which IEC device performance could be improved.

References

[1]G. Becerra, G. Kulcinski, J. Santarius and G. Emmert, "Design and Construction of a Neutral Particle Analyzer for an IEC Device", 15th US-Japan Workshop on Inertial Electrostatic Confinement Fusion, Kyoto University | Uji, Kyoto, Japan, 2013.

[2]C. Dietrich, "Improving particle confinement in inertial electrostatic fusion for spacecraft power and propulsion", Ph.D. dissertation, Massachusetts Institute of Technology, 1977.

[3]H. Eichhorn, K. Schoenbach and T. Tessnow, "Paschen's law for a hollow cathode discharge", *Applied Physics Letters*, vol. 63, no. 18, pp. 2481-2483, 1993. Available: https://www3.nd.edu/~sst/teaching/AME60637/reading/1993_APL_Schoenbach_et_al_hollow_cathode.pdf.

[4]R. Hirsch, "Inertial-Electrostatic Confinement of Ionized Fusion Gases", *Journal of Applied Physics*, vol. 38, no. 11, pp. 4522-4534, 1967. Available: 10.1063/1.1709162 [Accessed 15 May 2019].

[5]J. Khachan and S. Collis, "Measurements of ion energy distributions by Doppler shift spectroscopy in an inertial-electrostatic confinement device", *Physics of Plasmas*, vol. 8, no. 4, pp. 1299-1304, 2001. Available: https://aip.scitation.org/doi/pdf/10.1063/1.1349875?class=pdf. [Accessed 15 May 2019].

[6]M. Lieberman and A. Lichtenberg, *Paschen curves obtained for helium, neon, argon, hydrogen and nitrogen*. 2005.

[7]T. Lind´en, *Cross sections as a function of center of mass energy*. .

[8]T. McGuire, "Improved lifetimes and synchronization behavior in multi-grid inertial electrostatic confinement fusion devices", Ph.D. dissertation, Massachusetts Institute of Technology, 1977.

[9]G. Miley and S. Murali, *Inertial Electrostatic Confinement (IEC) fusion*. New York: Springer, 2014.

[10]T. Rider, "A general critique of inertial-electrostatic confinement fusion systems", Ph.D. dissertation, Massachusetts Institute of Technology, 1994.

[11]Pfeiffer Vacuum, 2019.

[12]J. Santarius et al., "Overview of University of Wisconsin Inertial-Electrostatic Confinement Fusion Research", 16th ANS Topical Meeting on Fusion Energy, Madison WI., 2004.

[13]A. Seltzman, "RTFTechnologies Mark 3 IEC Fusion Reactor", *Rtftechnologies.org*, 2005. [Online]. Available: http://www.rtftechnologies.org/physics/fusor-mark3-index.htm. [Accessed: 15- May- 2019].

[14]A. Seltzman, " Design of An Actively Cooled Grid System to Improve Efficiency in Inertial Electrostatic Confinement Fusion Reactors", Masters dissertation, Georgia Institute of Technology, 2008.

[15]A. Seltzman, "Welcome to Technical Plasmas LLC", *Technical Plasmas LLC*, 2018. [Online]. Available: https://techplasmas.com/. [Accessed: 15- May- 2019].

[16]M. William, “Development of Economic Spherical IEC Fusion Device”, Bachelors dissertation, Worcester Polytechnic Institute, 2015.

[17]R. Radev and E. Carlberg, "Longevity Tests of High-Sensitivity BD-PND Bubble Dosimeters", Lawrence Livermore National Laboratory, Livermore, 2019.

[18]"NRC: 10 CFR 20.1004 Units of radiation dose.", *Nrc.gov*, 2019. [Online]. Available: https://www.nrc.gov/reading-rm/doc-collections/cfr/part020/part020-1004.html. [Accessed: 16- May- 2019].

10 Acknowledgements

Many people helped make this work possible. First and foremost, I would like to thank Professor Anne White and Dr. Andrew Seltzman for allowing me to conduct this work, helping me with guidance, resources, and offering great feedback. I'm extremely grateful for the freedom afforded to me to in my time as a UROP student at the PSFC to pursue my passion for IEC fusion. I'm grateful not only for the wonderful opportunities afforded at the PSFC but also the ability to do real research in a real lab. I would also like to thank Willy Burke of the PSFC who worked alongside me to bring the fusor to the neatly packaged state that it is in today, and for answering whatever questions I asked. I would not have had the opportunity and ability to do this work without having had hands on experience with my own device prior to coming to the PSFC. To this end, I would like to thank Professor Michael Short who allowed me into his lab to work on my personal fusor since the start of my freshman year at MIT. It was in his lab that I learned the ropes of real research and developed the LabVIEW control that became a critical to the operation of the CCFD. I'm also grateful to Professor Short for allowing me into his lab once more while the old lab in which I worked was renovated. I would also like to thank Tom Toland of the PSFC who helped me work on the vacuum system of the CCFD and answer all my vacuum related questions. Finally, I would like to thank the folks of fusor.net for serving as an inspiration, a wealth of knowledge, and as a source of guidance for me since junior high on IEC related matters.

11 Appendix

1A Operation Manual for the CCFD

1. **<u>Preparation for Startup</u>**

    a. **Inspection Checklist**

        i. Inspect the following to ensure they are mechanically connected and not damaged:

            1) White high voltage cable from the back of the blue Spellman enclosure to the top of the vacuum chamber

            2) Green grounding cable from KF clamp connecting the blue convectron gauge to the blue Spellman enclosure.

            3) Gas lines near the cart handle

            4) Breaker capacity is 15A or greater.

2. **<u>Main Startup</u>**

    a. **Main Power**

        i. Ensure that power strip is turned on by verifying that convectron and physical control panel lights are illuminated.

        ii. Turn on laptop

    b. **Vacuum System**

        i. Looking from the back of the white Edwards roughing pump where the fan cage is visible, on the right of the chassis of the pump, press the power switch to turn on the roughing pump. Figure 1A. Has a red arrow pointing to this location.

        ii. Follow the hoses attached to the head of the roughing pump, identify the valve closest to the roughing pump (stainless steel body, black plastic cap). Unscrew this valve counter clockwise two full turns. Figure 1A. Has a green arrow pointing to this location.

iii. Following the same hose, you will come across a turbo pump, attached to it will be another valve labeled MDC, turn this valve one full turn counter clockwise. Figure 2A Has a blue arrow pointing to this location.

iv. Wait ~2 minutes and press the button labeled start/stop on the turbo pump controller on the front panel. You are waiting until the Convectron gauge reads around 800 mTorr. At that pressure, it is safe to turn on the turbopump. This will start the turbopump, to verify that the pump is responding, the front panel of the turbo controller will read "pump starting" and display the current rotation speed of the pump. *NOTE: pump rotation speed is not important as the system functions even if operated while the pump has not yet reached full rotational speed. Figure 3A Has an orange arrow pointing to this location.

c. Control System

i. The laptop password is cece

ii. On the desktop of the laptop, located a file called "best labview" Double click this file to launch the control program.

iii. Once labview is open, using the left click, navigate to the "manual control" tab of the VI. Once here, locate the slider labeled "Pressure mTorr". Below this slider will be an empty white box, take note of this box.

iv. In the upper left hand corner left click the play button to start the labview VI. A black arrow without any error popups indicates that the VI has started and is functioning properly. In the white box mentioned above in iii. Type 10 and hit enter on the keyboard.
*NOTE: You should now notice a green line has appeared on the right hand side graph. This is the setpoint line, i.e. the desired operational pressure for the system. A white line will also be present, and will fluctuate, this white line is the actual system pressure over time. The system has reached a stable state when the white and green lines overlap.

d. Gas System

i. Near the front of the cart, i.e. where the handle of the cart is located, there will be two gas bottles which serve as the fuel for the machine. The bottle nearest the turbo pump is argon and the other is deuterium. Locate the bottle with which you wish to operate, and identify its corresponding regulator by following the gas lines.

ii. Unscrew the bottle valve one full turn counter clockwise, then unscrew the regulator valve that corresponds to that bottle, until the gauge attached to the regulator reads between 5-20 psi.

*NOTE: the exact value doesn't matter, the control system functions regardless of input pressure if pressure is within the specified range.

e. Electrical System

i. From the back of the blue Spellman enclosure, near the power cable that feeds into it, locate the on off switch. Turn the enclosure power on.

ii. From the front of the supply adjust the current program dial to 99.9. This dial increases in value when turned to the right, and decreases to the left. If the reading is 0.00 and you cannot turn the dial further to the right, this means that it is already on 99.9 DO NOT ATTEMPT TO TURN FURTHER. Figure 4A. Has a white arrow pointing to this location.

iii. Similarly, turn the voltage program dial to read 50.0
*NOTE these values represent percent supply value, so for example, 99.9% of supply current is allowed when the dial is set to 99.9. For this model Spellman the current output may reach the 5 mA maximum that the supply is capable of. Similarly for voltage, a 50.0 value will allow the supply to reach 50% of its full voltage value, in the case of this supply, the voltage may reach 20kV on this setting. The supply is capable of 0-5 mA at 0-40kV. Figure 4A. Has a white arrow pointing to this location.

3. <u>Operation</u>

i. By now, the green setpoint line on the VI screen should be overlapping with the white real time system pressure line. If this is not the case, wait until this is the case. If system pressure has indeed reached setpoint, and is stable, then from the front panel of the blue Spellman enclosure, depress the orange button.

ii. At 10mA you should expect to visibly see a plasma formed in the vacuum chamber, but you should expect low voltage and high current draw. 1-2 kV or so is normal here as is 5mA.

iii. To increase system pressure, careful work your way down in 0.25 mTorr increments and allow the system pressure and voltage to stabilize to the new setpoint before proceeding. Because we start from 10 mTorr, these small increments result in very small changes (on the order of 100's of volts on the supply readout), but because the Paschen curve is exponential at low pressure, this is the only safe way to proceed when near 5 or so mTorr.
*NOTE: if you would intend to reach full system power, adjust the voltage dial from 50.0 to 99.9 before lowering pressure.

4. <u>Shutdown</u>

i. To shutdown the system first turn off the high voltage power from the switch on the back of the Spellman enclosure.

ii. Shutdown the turbo pump by pressing the start/stop button on the front panel of the turbo controller. The display should now read “pump ready” Once this is complete, close the valve connected to the turbo first, then the valve connected to the roughing pump, then both the gas bottle valves and the regulator valves.

iii. Set the pressure slider to 0 in the labview VI and ensure that the green setpoint line drops to 0. Shut off roughing pump via switch on side of pump. Once this is done, you may safely close the laptop down and shut off all system power from the power strip.

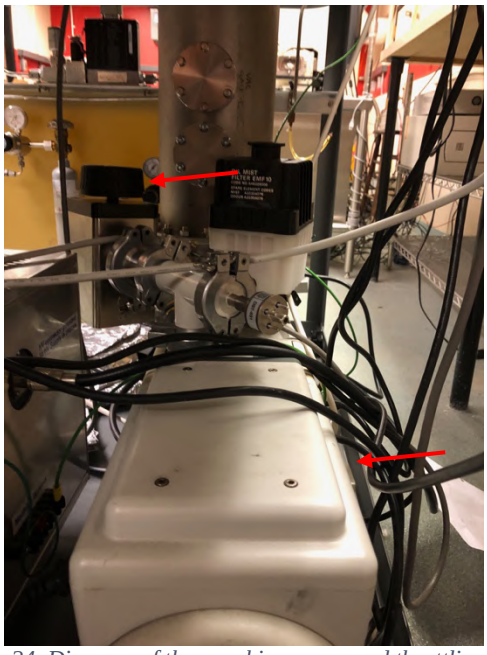

Figure 24. Diagram of the roughing pump and throttling valve.

Figure 2A. Digaram of the turbo pump and turbo throttling valve.

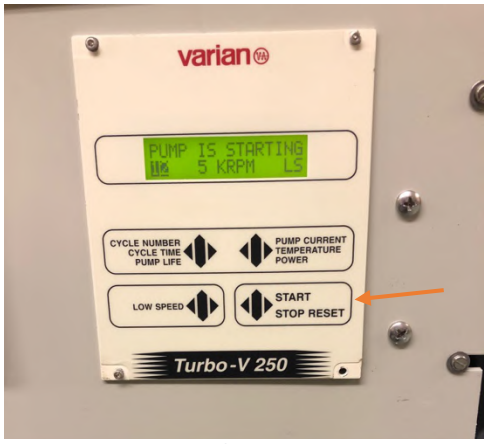

Figure 3A. Diagram of the turbo pump controller.

Figure 4A. Diagram of power supply control knobs.

2A Parts List

2A.1 Vacuum System

- NW200 Vacuum Chamber consisting of a 5 way cross, and long tube with many ports as outlined in figure 8.
- Edwards RV5 oil sealed rotary vacuum pump with oil mist eliminator, and kf25 fittings and hose to couple to turbo
- Varian V250 Turbotorr turbomolecular drag pump with corresponding controller and kf25 adapter to kf10
- Conflat adapter from turbo inlet to right angle 2.75” conflat throttling valve
- Granville-Phillips Mk 275 Covectron vacuum gauge
- MHV feedthrough for ion source
- High voltage feedthrough (alumina)
- Borosilicate viewport

2A.2 Gas Handling System

- Mass flow controller (10 SCCM MKS type)
- Multiple feet of ¼” stainless steel swagelok tubing and corresponding fittings / parts
- 15V + and – power supply for mass flow controller
- LabVIEW VI and USB-6001 DAQ
- Swagelok to 2.75” conflat adaptor
- Corresponding hydrogen and standard welding regulator for deuterium and argon respectively
- Gas manifold and “up to air valve in manifold”

2A.3 Power

- High voltage power supply (Spellman PVT40 series) capable of 40kV at 5mA packaged in Sparker enclosure
- Emco F40 power supply
- DC-DC converter for tuning input to EMCO supply
- MHV cable for ion source

2A.4 Detectors

- Ludlum model 177-61 bench top meter with model 44-21 probe
- 10XBTI 21-23 bubbles/mRem PND neutron dosmiters
- Ludlum Model 12 rate meter with 12” GE 3He proportional counter

2A.5 Controls

- I/O box with potentiometers and I/O with power connections
- LabVIEW VI

2A.6 Misc.

- Cart
- lead lined Shielding Boxes

3A Picture of Device

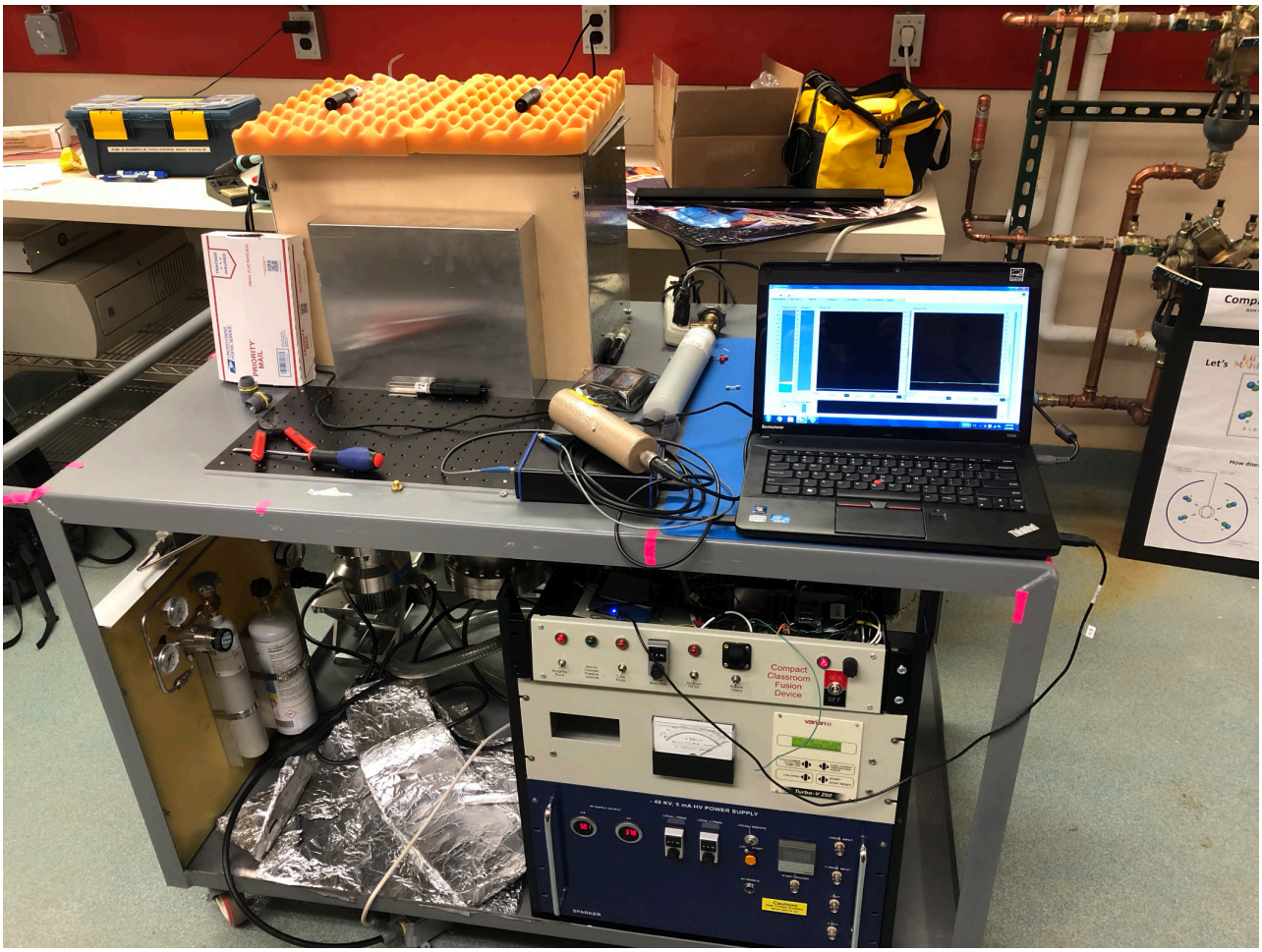

Figure 25. A picture of the CCFD.

4A Python Code Used to Calculate Flux and Error

```python
#Flux Calculator
import math

bubble_count = int(input("Enter bubble amount: "))
bubble_calibration = float(input("Enter a calibration value in bubbles/mrem: "))
detector_distance = float(input("Enter the detector distance from the grid in cm: "))
exposure_time = float(input("Enter an exposure time in seconds: "))

conversion_factor = bubble_count*28000 / exposure_time / bubble_calibration
isotropic_flux = conversion_factor * (4*math.pi * detector_distance**2)

#Error contribution calcs

detector_calibration_list = (21,21,21,22,23,23)
detector_calibration_mean = sum(detector_calibration_list) / len(detector_calibration_list)
calibration_error = 0.2

detector_calibration_error_contribution = (calibration_error * detector_calibration_mean) / detector_calibration_mean

time_error_contribution = 10 / 600
bubble_counts_error_contribution = math.sqrt(bubble_count) / bubble_count

detector_distance_error_contribution = 1

#Errors

conversion_factor_error_inverse = math.sqrt(detector_calibration_error_contribution**2 + time_error_contribution**2 + bubble_counts_error_contribution**2)
conversion_factor_error = conversion_factor_error_inverse**-1

total_error_inverse = math.sqrt(conversion_factor_error**2 + 2*(detector_distance_error_contribution**2))
total_error = (total_error_inverse**-1) * isotropic_flux

print("-------------------------------------Results-------------------------------------")
print("The isotropic neutron flux is:", isotropic_flux, "+/-" , total_error)
```

Figure 26. Python Code used to calculate flux and error.